



PCCP

How Does Hydrogen Bond Network Analysis Reveal the Golden Ratio of Water-Glycerol Mixtures?

Journal:	<i>Physical Chemistry Chemical Physics</i>
Manuscript ID	CP-ART-11-2019-006246.R1
Article Type:	Paper
Date Submitted by the Author:	16-Dec-2019
Complete List of Authors:	Fisher, Trevor R; University of Oklahoma Zhou, Guobing ; University of Oklahoma Shi, Yijun; Lulea University of Technology Huang, Liangliang; University of Oklahoma

SCHOLARONE™
Manuscripts

How Does Hydrogen Bond Network Analysis Reveal the Golden Ratio of Water-Glycerol Mixtures?

Trevor R. Fisher,[†] Guobing Zhou,[†] Yijun Shi,[‡] Liangliang Huang*,[†]

[†]School of Chemical, Biological and Materials Engineering, University of Oklahoma, Norman, Oklahoma 73019, United States

[‡]Division of Machine Elements, Luleå University of Technology, Luleå, 97187, Sweden

Abstract

Properties of water-glycerol mixtures depend closely on the water/glycerol ratio. Around the 30 mol% glycerol concentration, the so-called golden ratio of water-glycerol mixtures, several of the mixture's properties have an observed maxima or minima, without a clear fundamental explanation. In this work, a series of molecular dynamics simulations have been performed over a wide range of water-glycerol concentrations to analyze the intermolecular hydrogen bond (H-bond) network. The collected values from simulations are justified from both a probabilistic model of H-bonding and from observing the dynamic behavior of each type of H-bonds. The populations of H-bonds that exist at a given concentration of glycerol are largely governed by the probability of one oxygen atom randomly associating with another oxygen atom. However, the H-bonds that glycerol oxygen can form are dependent on the H-bonds that are formed by the other intramolecular glycerol oxygen. Based on the dynamic analysis of each type of H-bonds, there are deviations from randomly associating with another oxygen. Water preferentially donates a hydrogen to a glycerol than to another water molecule. Yet, glycerol has a near-equal likelihood for donating a hydrogen to either another glycerol or a water. This has an effect of increasing the number of H-bonds between water and glycerol molecules and decreasing H-bonds between two water molecules. A maximum contribution of H-bonds between water and glycerol occurs around 30 mol% glycerol which is a concentration where several of the mixture's properties have an observed maxima or minima.

1. Introduction

Water-glycerol mixtures are used for a variety of applications due their unique properties that cannot be obtained from either pure substance. One of the unique properties of the mixture is that it hinders crystallization. Adding glycerol to water depresses crystallization of water even at temperatures below the homogeneous nucleation temperature of pure water, which allowed for the observation of a liquid-liquid transition that cannot be experimentally accessed for pure water [1]. The mixture has a minimum freezing point at 66 wt% glycerol, far lower than the freezing point of either pure solution [2]. This makes water-glycerol mixtures a good antifreeze component. Interestingly, another property of the mixture reaches a maximum around the same concentration of glycerol: the volume contraction coefficient, which is related to the deviation from ideal mixing, has a maximum that occurs around 60 wt% glycerol [3].

It has also been proposed that the water-glycerol mixture can be used as a superlubricant between two hydrotreated surfaces. In a study by Matta et al., a friction coefficient lower than 0.01 is achieved between two sliding surfaces of tetrahedral amorphous carbon (ta-C) lubricated by glycerol [4]. Normally, low friction is created by a self-assembled monolayer (SAM) of polar molecules with long aliphatic chains [5]. But neither water nor glycerol has the molecular structure to create a SAM. Instead, the H-bond network is proposed to explain the anomalous low friction observed for a water-glycerol lubricant. Tribodegradation of glycerol between the sliding plates hydroxylates the ta-C to create a hydrophilic surface capable of promoting the H-bond network. Additionally, a low viscosity, thin nanolayer of water would be generated as a product of glycerol tribodegradation to further enhance superlubrication. The hydroxylation of ta-C via tribochemical reactions was confirmed by an additional study [6]. Molecular dynamics (MD) simulations further revealed that glycerol is also undergoing tribochemical degradation to form acids and water. However, neither the presence nor the role that a water nanolayer has on creating the superlubrication regime has been directly proven.

Presently, the role that H-bonds have on improving lubrication and their relation to the property minima/maxima occurring around 60 wt% glycerol would like to be better understood for water-glycerol solutions. In this work, the contributions of different H-bonds in water-glycerol solutions as well as their dynamic properties are examined over a wide range of glycerol concentrations. Through molecular dynamics simulations, individual H-bonds can be directly identified to count the populations in each system and tracked over time to observe the rate that

H-bonds disassociate. Those measurements could provide a benchmark for the behavior of H-bonds in the presence of dilute and concentrated amounts of glycerol. It is worth pointing out that hydrogen bond statistics and dynamics of pure water has helped explain the non-Arrhenius temperature dependence of bulk water properties at supercooled temperatures above the homogeneous nucleation temperature [7, 8, 9]. As the temperature decreases to the homogeneous nucleation temperature, the number of hydrogen bonds in water increases which restricts molecular diffusion. Despite the non-Arrhenius behavior of diffusive bulk properties of water at low temperatures, the molecular rotations corresponding to H-Bond breaking and formation in water maintained a normal Arrhenius relationship. For water-glycerol solutions, studying the H-bond statistics and dynamics can provide more fundamental insight for why several of the mixture's properties have a maxima/minima occurring around 60 wt% glycerol.

Some H-bond statistics for the water-glycerol model used in this study have already been measured in previous experiments and simulations. For example, in previous MD studies, the number of each type of H-bonds was counted in water-glycerol solutions at low temperatures under glass-phases and for pure glycerol at moderate temperatures from 250-400 K [10, 11]. Analyses of H-bonds have also been performed for 0-30 mol% glycerol solutions [12] and at 80 mol% glycerol [13]. Based on a model validation study of different water-glycerol models used in MD simulations [14], the water-glycerol model used in ref. [11], which is also the model adopted in this study, can more accurately predict the experimental bulk thermodynamic properties of water-glycerol mixtures. In this study, radial distribution functions (RDF's) and angle distribution functions (ADF's) are calculated in order to determine appropriate geometric definitions for H-bonds at different concentrations. After the geometric H-bond definitions are justified, the fraction of each type of H-bond in the water-glycerol system as a function of glycerol concentration is analyzed for an observed maximum occurring around 60-70 wt% (~23-31 mol%) glycerol. We develop a new approach to verify that the fractions of each type of H-bond observed from MD results can be justified based on entropic effects and preferred conformations. Through a probability model, we describe how oxygen randomly associating with another oxygen could account for entropic effects. In addition, the dynamic relaxation of H-bond populations is examined to determine if certain H-bond conformations are preferred over others.

2. Models and Simulation Details

2.1. Molecular Dynamics Simulation Details

Molecular dynamics simulations are performed using the open-source LAMMPS software version released on August 22, 2018 [15, 16]. LAMMPS is able to perform time integration of atomic particle movement based on the energy potentials that are specified for a molecular system. The details for the time integration and equations of motion are available in ref. [17]. For the water-glycerol systems studied, the contributions to the total energy of the system include Lennard-Jones interactions, electrostatic Coulombic forces, bond strain, angle strain, and dihedral strain. The choice of these contributions is to comply with the water-glycerol model used in ref. [14]. The Lennard-Jones interactions are an attractive force at long ranges to simulate van der Waals (VDW) interactions and repulsive at close range to account for electron orbital repulsion. The Lennard-Jones potential is calculated from:

$$E_{VDW}(r) = LJ(r) = 4\epsilon \left[\left(\frac{\sigma}{r} \right)^{12} - \left(\frac{\sigma}{r} \right)^6 \right] \quad r < r_c \quad (1)$$

$$E_{VDW}(r) = LJ(r) * S(r) \quad r_c < r < r_{\max} \quad (2)$$

$$E_{VDW}(r) = 0 \quad r > r_{\max} \quad (3)$$

Where ϵ corresponds to the strength of the van der Waals attraction, and σ indirectly modifies the distance where the lowest energy occurs between two atoms by defining the distance where the Lennard-Jones energy is zero between two atoms. The Lennard-Jones contributions are calculated between all atoms within a distance r_c from each other. Past this distance, the calculated energy is very small but not 0. In order to smooth out the transition in energy from $E(r_c)$ to zero, a force-switching function, $S(r)$, is used between r_c and a larger radius r_{\max} to scale the calculated energy to zero [18]: $S(r) = \frac{(r_{\max}^2 - r^2)^2 (r_{\max}^2 + 2r^2 - 3r_c^2)}{(r_{\max}^2 - r_c^2)^3}$. For most calculations in this study, r_c is set to 11 Å and r_{\max} is set to 12 Å in compliance with ref. [14]. The system at 300 K and 70 mol% glycerol used a Lennard-Jones cutoff at 12 Å and no switching function was used for approximately 70 ns of equilibration. Then, the switching function was implemented for the system. The effects of

using a switching function on these systems are determined to be negligible, see the discussion in the Appendix.

Coulombic interactions between two atoms i and j are modeled by

$$E_Q(r) = \frac{Cq_iq_j}{\epsilon_{dp}r} \quad r < r_{max} \quad (4)$$

where C is an energy-conversion constant, ϵ_{dp} is the dielectric permittivity, and q_i and q_j are the charges of atoms i and j , respectively. For atom pairs closer than r_{max} , the Coulombic attractions are calculated directly. The Coulombic attractions from the contributions of atoms farther than r_{max} are approximated using a particle-particle particle-mesh solver in reciprocal space [19]. It maps atom charges to a 3D mesh and uses FFT's to solve Poisson's equation. The electric field generated on the 3D mesh is used to determine the additional long-range Coulombic attractions for each atom. A damping factor is applied to the direct Coulombic attractions to account for the contribution of nearby atoms to the electric field. For all calculations in this study, r_{max} for direct Coulombic interactions was 12 Å.

The energy of bond strains and angle strains are calculated by a harmonic oscillator

$$E_b(r) = K_b(r - r_o)^2 \quad (5)$$

$$E_\theta(\theta) = K_\theta(\theta - \theta_0)^2 \quad (6)$$

Where K_b and K_θ are spring constants and r_o and θ_o are the equilibrium bond length and bond angle, respectively.

The energy of dihedral strains is calculated by

$$E(\phi) = K_\phi[1 + d\cos(n\phi)] \quad (7)$$

Where d is either 1 or -1, K_ϕ is a spring constant, and n corresponds to how many stable angles the dihedral can conform to. The angle of the dihedral, ϕ , is scaled such that 0° corresponds to the cis conformation.

The values for the parameters of glycerol molecules can be found in the supplementary information for ref. [10], and the parameters used for water are the TIP4P/2005 model found in ref. [20]. Only the parameters for Lennard-Jones interactions between the same atom type are given in the above references. For Lennard-Jones interactions between different atom types, the Lorentz-Berthelot mixing rule is used

$$\sigma_{ij} = \frac{\sigma_{ii} + \sigma_{jj}}{2} \quad (8)$$

$$\epsilon_{ij} = \sqrt{\epsilon_{ii}\epsilon_{jj}} \quad (9)$$

All H-bond analyses from the MD simulations, including geometric distribution functions, H-bond identification, and H-bond dynamics, are performed with in-house code.

2.2. Water-Glycerol Model Validation

The initial development of the glycerol model used in this study was performed by Chelli et. al [21]. In the study, Lennard-Jones, bond, angle, and dihedral force field parameters were obtained from the AMBER force field [22]. The atomic charges were determined by an electrostatic potential fit using *ab initio* quantum mechanical calculations at the B3LYP/6-31G* level. The molar specific heat, density of states, and radial distribution functions were calculated based on molecular dynamics simulations and compared to experimental data, for example, the density of states from incoherent neutron scattering.

The charges and Lennard-Jones parameters of the hydrogen atoms in the glycerol model were modified in ref. [23] in order for the diffusion from MD simulations to more closely match experimental results. The relaxation time obtained from intermediate structure factor analysis also agreed with the relaxation time calculated from coherent neutron scattering experiments [24]. The model proposed in ref. [23] was compared against 4 other models for glycerol by measuring various bulk thermodynamic properties as a function of temperature [10]. The density, thermal expansion coefficient, and diffusion agreed well with experiments, but the heat capacity at constant pressure, along with all other models, was twice as large as the value from experiments. Validations of glycerol models with different water models have been also performed [14]. In

conclusion, the glycerol model combined with the TIP4P/2005 model for water [20] was best able to replicate the temperature and concentration dependence of bulk thermodynamic properties of water-glycerol mixtures.

3.3. Initial Structure and Simulation Equilibration

All simulations performed consist of 1464 molecules with varying concentrations of glycerol. A total of 5 different molar concentrations of glycerol, 0.068%, 10%, 30%, 50%, and 70%, are studied to observe how hydrogen bonds will change in the presence of either dilute or saturated glycerol mixtures. The 0.068 mol% glycerol mixture contains a single glycerol molecule with 1463 water molecules and is referred to as < 1 mol% glycerol throughout this study. It is worth noting that for this lowest concentration of glycerol investigated, the analyses of radial distribution function (RDF, Figures 5 and 7), the angle distribution function (ADF, Figure 6) and the hydrogen bond definition (Tables 2) and kinetics (Table 3) are performed only to water-water pairs. The initial structures for the water-glycerol mixtures are prepared using the PACKMOL code to randomly place water and glycerol molecules in a simulation volume without molecular overlap [25]. The appropriate starting volume to place the molecules is based on standard mixing rules for water and glycerol at STP. Values of the specific gravity for water-glycerol mixtures given in ref. [26] indicate that standard mixing rules will give a reasonable starting volume. The dimensions of the initial cubic simulation boxes range from 35 Å³ to 52 Å³ depending on the molar concentration of glycerol. Initial velocities are assigned to atoms in the system by randomly sampling from a gaussian distribution of velocities corresponding to a temperature of 300 K. Velocities are assigned in such a way that there is no net momentum or rotation of the system. Time integration of the system is performed using a constant NPT ensemble using the equations of motion described in ref. [17]. The time between integration steps is 1 fs in accordance with the model verification study in ref. [14]. Pressure is set to 1 bar and controlled by a Nose-Hoover barostat with a damping parameter of 1ps. Temperature is set to 300 K and controlled by a Nose-Hoover thermostat with a damping parameter of 0.1 ps. Periodic boundaries are set for all 3 dimensions. System equilibration is allowed to take place over 20 ns for all water-glycerol mixtures. For higher concentrations of glycerol, the glycerol molecules have a diffusion coefficient of O(10⁻⁷ cm²/s) [14], so glycerol will travel around 11 Å on average over 20 ns.

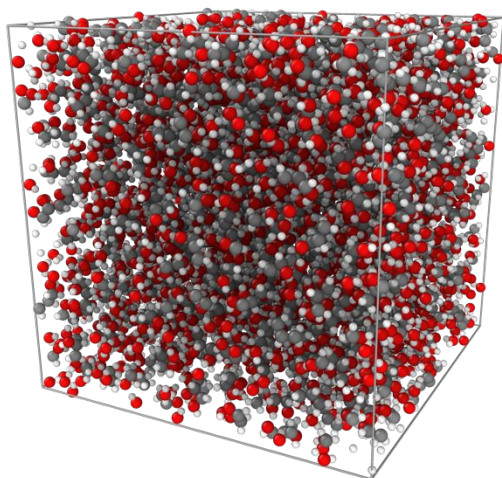


Figure 1. – Example of a typical water-glycerol simulation cell. A 50 mol% glycerol solution after 20 ns of equilibration at 300K and 1 bar is shown. Image of the molecular system is generated with OVITO software [46].

Equilibration of the water-glycerol systems is estimated by observing the time-dependence of the total energy and density of the system. Both density and total energy of the systems converge within approximately 4 ns. For the 50 mol% glycerol solution, the average total energy of the system is -2860 eV with a standard deviation from the average of ± 5.82 eV based on values measured every 1 ps from 4 ns to about 20 ns after the start of the simulation (Note: this energy value is extensive and not normalized to a molar basis). This standard deviation corresponds to a relative deviation from the average of 0.2% which suggests stable behavior in the system from 4 ns to 20 ns.

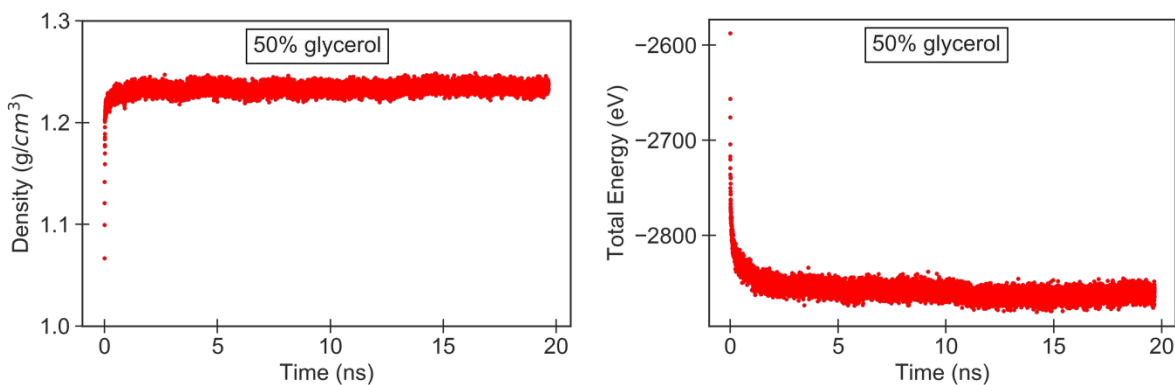


Figure 2. Changes in density (Left) and total energy (Right) as the initially generated molecular structure relaxes to a lower energy.

3. Results and Discussions

3.1. Hydrogen Bonds in Water-Glycerol Mixtures

For a system containing water and glycerol molecules, the only atoms that are considered to form H-bonds are the oxygen atoms and their covalently bonded hydrogen atoms. There are 4 possible types of intermolecular bonds considered based on combinations of donor-acceptor atoms, see Table 1.

Table 1. Intermolecular hydrogen bond definitions.

Abbreviation	Donor Atom	Acceptor Atom
g-g	Glycerol oxygen (O_g)	Glycerol oxygen (O_g)
w-w	Water oxygen (O_w)	Water oxygen (O_w)
g-w	Glycerol oxygen (O_g)	Water oxygen (O_w)
w-g	Water oxygen (O_w)	Glycerol oxygen (O_g)

For glycerol, it is possible for intramolecular H-bonds to form [10, 11]. Across a wide temperature range and in both dilute and concentrated amounts of glycerol, glycerol molecules contain around one intramolecular H-bond on average. However, in this study, only the intermolecular H-bonds of the mixtures will be measured. As indicated from the above studies, the number of intramolecular glycerol H-bonds remains nearly constant across all concentrations of glycerol and only provide a small contribution to the total number of H-bonds per glycerol molecule (around 7-8). The presence of intramolecular H-Bonds will reduce the number of intermolecular bonds for glycerol oxygen, but their dynamic properties are not estimated to be much different from intermolecular g-g H-bonds due to the identical interaction parameters. This is, however, an assumption and future research may wish to analyze the dynamic properties of intramolecular H-bonds in water-glycerol mixtures.

The central oxygen atoms could be distinguished from the oxygens connected to the terminal carbons in glycerol based on different steric hinderances. However, the Coulombic and Lennard-Jones parameters used to define the glycerol oxygen atoms in the molecular simulations are identical and it is expected that the dynamic properties will not differ greatly. From studies of the water-glycerol mixture at low temperature, the structural order between terminal and central oxygen atoms and water atoms is similar based on radial distribution function analysis [11].

Nevertheless, it should be noted that all static and dynamic parameters obtained for H-bonds containing glycerol have contributions from both terminal and central oxygen atoms.

3.2. Measuring Hydrogen Bonds in Experiments

In experiments, hydrogen bonds can be identified by frequencies corresponding to OH bond stretching. However, the dynamical breaking and reforming of hydrogen bonds cannot be measured directly, only correlated. From the vibrations of OH bonds, the contribution of the faster liberation motions can be separated out from the frequency distribution and correlated to hydrogen bond dynamics [7]. A few examples of studying OH bond vibrations in either water or glycerol include Rayleigh light scattering [30, 31], dielectric relaxation [32, 33], incoherent quasielastic neutron scattering (IQENS) [34, 35], and coherent quasielastic neutron scattering (QENS) [7, 24]. The faster liberation motions identified through IQENS and QENS on light and heavy water correlate to rotation of hydrogen about the center of mass of molecules [7]. This motion is referred to as β relaxation. For water, β relaxation is assumed to correlate strongly with hydrogen bond breaking and reformation. A comparison of the temperature dependence of the β relaxation extrapolated from several experimental methods and the hydrogen bond dynamics obtained from molecular dynamics simulations shows activation energies ranging from 8 to 11 kJ/mol and an agreement on absolute values of the dynamic rates within an order of magnitude [7]. This gives some confidence that hydrogen bond dynamics measured in simulations can be compared with isolated vibrational frequencies obtained from experiments. However, it is outside of the scope of this paper to discuss or determine the methodology of identifying a separable vibrational frequency that would correspond to glycerol H-bonds in water-glycerol solutions, nor is it known by the author if such an approach is currently feasible. Up to this point, coherent and incoherent neutron scattering experiments have been performed on glycerol solutions [24, 35]. From the incoherent neutron scattering experiments, motions related to diffusive and structural relaxation have been isolated, but H-bonding is only one component of the structural relaxation of glycerol.

3.3. Assigning H-Bond Criteria for Molecular Simulations

In this study, a geometric criteria with a maximum radius between the donor and acceptor oxygen is used along with an angle criteria for the donor-hydrogen-acceptor configuration, see Figure 3. The maximum radii used for different H-bonds are based on radial distribution functions between

the specified donor-acceptor pair, and the angle criteria is specified such that the donor-hydrogen-acceptor bonds form a near linear chain.

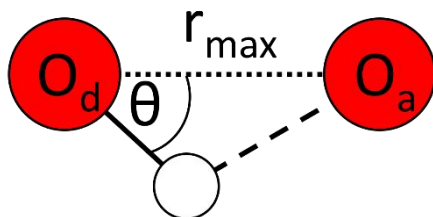


Figure 3. Geometric hydrogen bond definition employing a maximum distance between the donor oxygen (O_d) and acceptor oxygen (O_a), r_{max} , and a maximum angle, θ , between the O_d - O_a vector and O_d -H bond.

A radial distribution function (RDF) between a central and terminal atom calculates the relative density of terminal atoms, $g(r)$, at a given distance, r , away from a central atom compared to the average density of the terminal atom throughout the entire system. RDF analysis is used to probe the structural order in systems based on the location and intensity of the peaks. Larger peaks at a given distance indicate that central and terminal atoms have a higher probability to be separated by the corresponding distance and suggests a structural ordering of the particles. Because the value of $g(r)$ is normalized to the bulk density, the value of $g(r)$ will approach unity at large distances of r corresponding to an unordered association between the central and terminal particles.

RDF's are calculated by averaging $g(r)$ over all of the central atoms in a simulation system as well as averaging over 500 timesteps separated by 40 fs for the system containing 0.068 mol% glycerol and 10 ps for the other systems. Only the specified terminal atoms contribute to the value of $g(r)$, and intramolecular atoms are also excluded from the RDF calculations.

A standard RDF calculated with glycerol oxygen as the central atom is affected by the obstruction of the carbon backbone of the glycerol molecule. The first peak corresponding to H-bonded neighbors is diminished due to the smaller accessible area around the central glycerol atom. A standard RDF assumes that the entire volume of a finite radial shell is available for terminal atoms to occupy, but this is not the case for small distances around a glycerol oxygen. To account for the obstruction of the glycerol backbone, a previous study that performed MD simulations of water-glycerol solutions employed a "half-volume" RDF [11]. A plane was defined orthogonally

to the C-O bond on the central oxygen atom that split the simulation box into two sides. The RDF was calculated only on the half of the simulation box that excluded the carbon backbone. To achieve a similar effect, an angle is assigned between the central glycerol oxygen, the covalently bonded carbon, and the neighboring oxygen. If this angle is less than 90° , then the neighboring oxygen is on the carbon backbone half of the simulation box and is excluded from the RDF calculation.

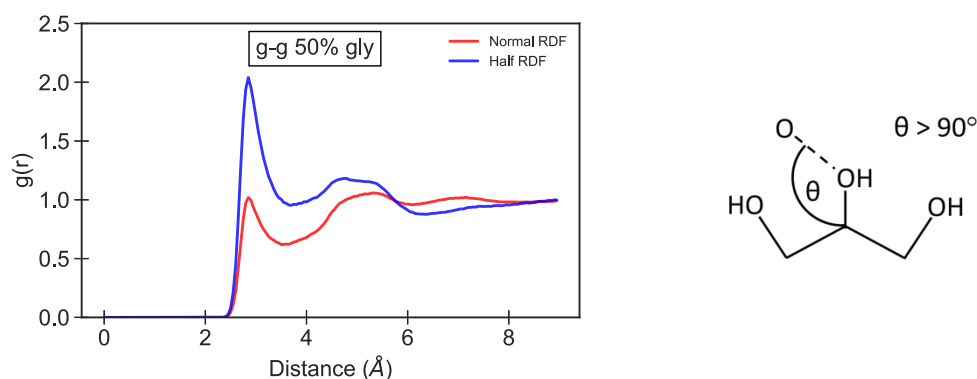


Figure 4. (Left) Standard RDF compared to a “half volume” RDF with glycerol atoms as both the central and terminal atom for a 50 mol% glycerol mixture. (Right) Illustration of how an oxygen-oxygen pair is determined to be included in the “half volume” RDF.

From Figure 4, the obstruction of the glycerol backbone affected the normal RDF between glycerol oxygen by reducing the apparent correlation in the first and second solvation shell. The “half volume” RDF restores the peaks corresponding to the first and second solvation shell and slightly shifts the location of the first peak to a farther distance. In order to more clearly see the correlation between glycerol oxygen and other oxygen atoms, the RDF’s calculated with glycerol as the central atom in Figure 5 utilize a “half volume” RDF.

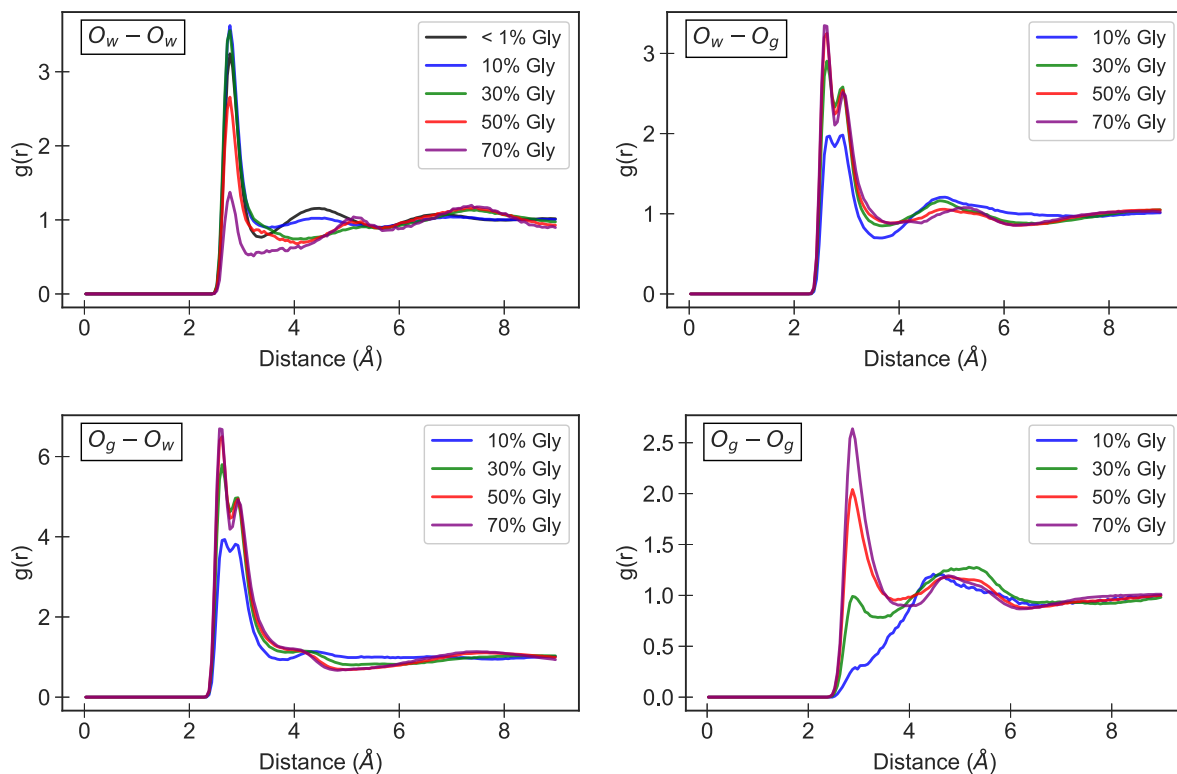


Figure 5. RDF's between the different specified oxygen pairs. The first letter indicates the central atom and the second letter indicates the neighbor atom in the RDF. O_w-O_w and O_w-O_g RDF's are calculated normally and O_g-O_g and O_g-O_w RDF's are calculated using a half-volume RDF to account for the obstruction of the carbon backbone on the RDF calculation.

The RDF between all combinations of water and glycerol oxygen pairs are calculated to determine the distances that H-bond donor and acceptor atoms are separated by. The first peak between oxygen atoms corresponds to the closest neighbors which are candidates for H-bonding. The width of the peaks corresponds to the vibrational freedom of the H-bonds and result in a range of possible H-bond distances.

Overall, the location of the first peaks for oxygen-oxygen RDF's in water-glycerol systems are not influenced by the glycerol concentration, but the width and strength of these peaks are. The correlation between O_w decrease as the glycerol concentration increases which indicates that, while the distance between O_w does not change, there are fewer instances of O_w neighboring each other. A similar conclusion can be made for O_g as the glycerol concentration decreases. This is expected as it is statistically more likely for an oxygen atom to associate with the opposite molecule as the opposite molecule's concentration increases. However, it is interesting to note that even at 30

mol% glycerol, a concentration where there are more glycerol oxygen atoms than water oxygen atoms, there is still a very low frequency of O_g-O_g neighbors.

The second peak in the O_w-O_w RDF is also lowered at glycerol concentrations of 30 mol% and above. The second peak, appearing around 4.5 Å, is characteristic of the second hydration layer in ordered hexagonal ice [36]. This suggests that higher glycerol concentrations disrupt the ordered network of H-bonds normally present in pure water. The disruption of the pure water H-bond network with increasing glycerol concentration may be responsible for reducing the melting point of the mixture compared to a pure water solution. These changes in the water network with increasing glycerol concentration are similar to what was observed in the liquid-liquid transition of a dilute water-glycerol mixture in the supercooled regime [11]. They observed that water molecules transitioned from the second hydration layer to the first when water transformed from a low density amorphous (LDA) liquid to a high density amorphous (HDA) liquid. However, in the case of increasing glycerol concentration, the first hydration layer peak broadens but the number of neighbors in the first hydration peak decreases instead of increases.

The first peaks in the RDF's between glycerol oxygen and water oxygen (O_g-O_w and O_w-O_g in Figure 5) are very similar over the range of 30 mol% to 70 mol% glycerol and suggests a similar number of glycerol-water oxygen neighbors across this concentration range. The double peak suggests two different preferred distances, and this turns out to be due to which oxygen atom is donating a hydrogen to the other oxygen (See Figure 7). This double peak was also identified in the RDF's of dilute water-glycerol mixtures in the supercooled regime in ref. [11].

The distance of the first minimum after the first peak in each RDF is used to specify an initial cutoff distance to further analyze the orientation of water and glycerol oxygen neighbors using an angle distribution function (ADF), which is similar to a RDF except it measures the frequency of $\angle O_dHO_a$ angles, $g(\theta)$ (this angle is identical to the one defined in Figure 3). The values of $g(\theta)$ are not normalized based on the different volumes of $g(\theta+\Delta\theta)$ because the purpose of the ADF in this study is to compare "at face value" the number of H-Bond pairs detected at different angles and ultimately specify a reasonable maximum H-Bond angle that would incorporate a majority of the H-Bonds. Specifying too small of a cutoff angle for H-bonds would only identify a small fraction of the entire "true" H-bond population in a system. Too large of a cutoff angle would overestimate H-bond populations by incorporating a significant number of false positive H-bonds. By looking at the ADF's for each type of H-bond, an ideal angle can be selected

for each type of H-bond that will include most of the H-bonds without including too many false negative H-bonds. For ADF functions with water oxygen as the central atom, two angles are calculated for every specified neighbor to calculate the angle between the terminal oxygen and each hydrogen atom bonded to the water oxygen.

For all of the ADF's measured, the peaks emerging at low angles and high angles correspond to the central atom donating and accepting in a H-bond, respectively. In the first case, the angle between the central atom's covalently bonded hydrogen and the neighbor atom is small and suggests that an H-bond is formed by donating its hydrogen to the neighbor. When the measured angle is large, the central atom's hydrogen is pointed away from the neighboring atom to allow for it to associate with the neighbor's hydrogen atom. For both water and glycerol oxygen atoms, the preferred angles between their neighbors and hydrogen atoms are independent of whether the neighbor is a water or glycerol oxygen. This can be seen by similar peaks occurring in the ADF's in Figure 6 that have the same central atom.

However, water and glycerol oxygen atoms have slightly different ranges of angles that correspond to donating or accepting a hydrogen from its neighbor. The small measured angles in the w-w and w-g ADF, corresponding to H-Bonds with water oxygen as the donator atom, fall below 30° - 35° . The exception to this generalization is a broader range of angles associated with w-g H-Bonds at 10 mol% and 30 mol% glycerol. In the cases where water oxygen has its hydrogen oriented away from the neighbor atom, the angle is slightly over 100° . This angle occurs when the other hydrogen attached to the water oxygen is oriented towards the neighbor atom and when both hydrogens are oriented away from the neighboring atom.

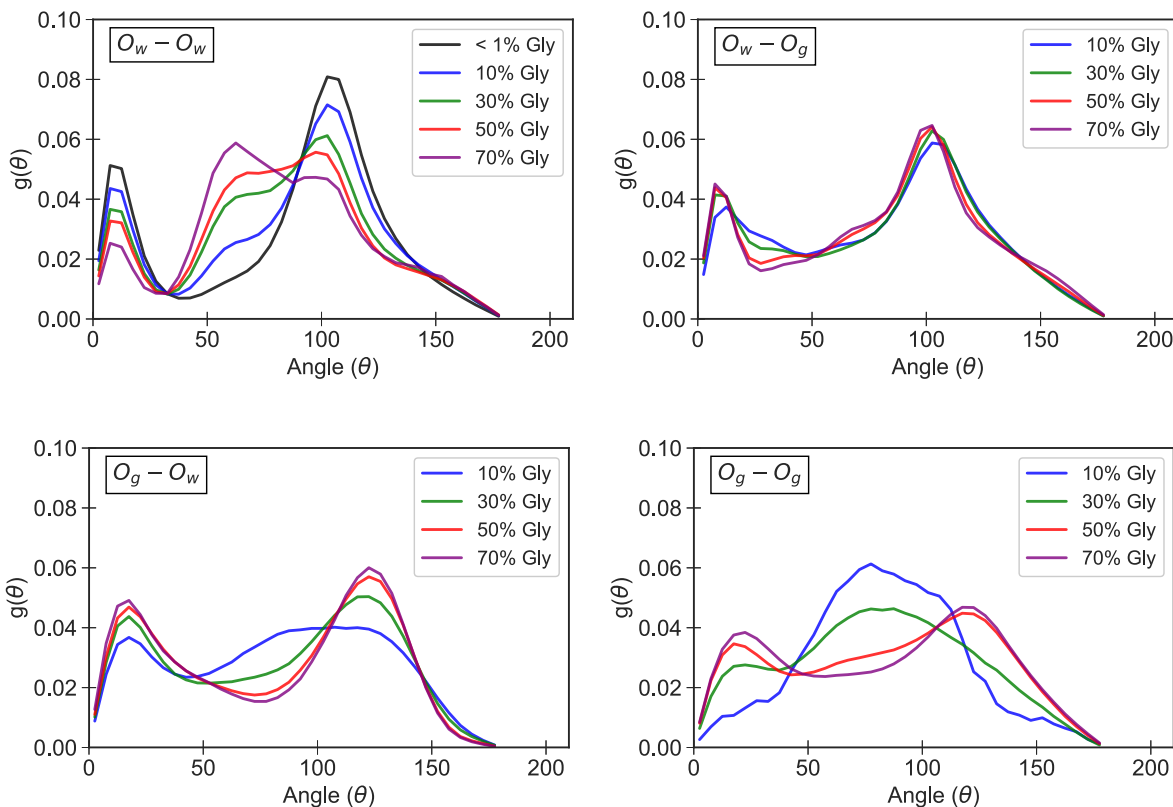


Figure 6. ADF's between the different specified central-neighbor oxygen pairs and the hydrogen atoms attached to the central atom. The measured angle, θ , is the angle defined in Figure 3. Values of $g(\theta)$ are normalized by the total number of angles measured to allow for comparison between different glycerol concentrations. Thus, the value of $g(\theta)$ is the fraction of neighbors for a given system that form an angle θ with the central atom's hydrogen.

For glycerol oxygen, the peak associated with hydrogen donation is broader and extends out around 50° - 70° . This is consistent with ref. [10] where it was stated that internal interactions will cause the glycerol-glycerol H-bond angle to be larger than 20° . The preferred angle formed when the central glycerol is accepting a hydrogen bond from the neighbor atom is around 125° . Because glycerol oxygen only has 1 hydrogen atom, the single hydrogen is able to distance itself farther from the neighbor hydrogen than the two hydrogen on water oxygen.

A caveat when analyzing the g-g ADF at low concentrations is that the parabolic distribution with a maximum of 90° is an artifact of not normalizing $g(\theta)$ based on the volume of $g(\theta+\Delta\theta)$. If the values of $g(\theta)$ were to be normalized based on the volume of each angle bin, then

the values of $g(\theta)$ would show a near uniform density for all angles of θ and only a slight preference for the angles corresponding to hydrogen donating and accepting at higher glycerol concentrations.

An interesting feature of the w-w ADF is a peak occurring at around 60° that becomes more prominent with increasing glycerol concentration. This is neither a small angle associated with hydrogen donation nor an artifact of the difference in the volumes of the angle bins. The water oxygen neighbors with a $\theta = 60^\circ$ could be due to crowding of non-H-bonded water molecules. A possible explanation is neighboring water molecules that are H-bonded with two different intramolecular glycerol oxygen get constrained closer together as increasing glycerol concentrations reduce the accessible space for water domains.

The following HB analysis requires a reasonable maximum H-bond angle to be specified for each donor-acceptor pair. Due to molecular vibrations, no H-bond configuration will be completely linear, and an angle tolerance is selected based on ADF's of donor-acceptor atoms to ensure that a majority of the "true" H-bond population is identified without including too many false positive H-bonds. The H-bond angle is specified to be less than 35° for H-bonds with water oxygen as the donor atom and 50° for H-bonds with glycerol oxygen as the donor atom. These angles are based off of the minima that occurs after the first peak in the w-w ADF in the <1 mol% glycerol solution and in the g-g ADF for the 70 mol% glycerol solution, respectively. The location of the minima does shift with changing glycerol concentration as well as for the w-g and w-g ADF's. However, the shifts are very slight due to changing glycerol concentrations. The most dramatic change in the minima occurs in the g-w ADF, shifting up to 75° at higher glycerol concentrations. However, based on the observation of water crowding at higher glycerol concentrations, the broadening of the first peak could be due to more tightly packed water molecules that are associated with another intermolecular glycerol oxygen. Including these additional tightly packed water molecules would be introducing false-positive g-w H-bonds, so the smaller angle cutoff of 50° is maintained for all H-bonds with glycerol oxygen donors.

3.4. Determining Number of Hydrogen Bonds in a Water-Glycerol System

In order to determine a more appropriate maximum radius for H-bonds, a modified RDF that imposes the H-bond angle criteria is calculated for each donor-acceptor pair, $HB(r)$. The central atom in the modified RDF calculation is treated as the donor atom in a H-bond and the neighbor atom is the acceptor atom. For each hydrogen bonded to the central atom, the angle is checked

between the central atom, hydrogen, and neighbor. If the angle is less than the maximum angle specified from the ADF analysis, then it is included in $HB(r)$. With the added angle constraint, the $HB(r)$ for a central-terminal pair, O_c-O_t , measures the type of H-bond with a donor-acceptor pair of d_c-a_t .

When $HB(r)$ is integrated up to the maximum radial cutoff for a H-bond, this will yield the average number of a given type of H-bond per donor atom. The H-bond angle is based on the ADF analysis performed in the previous section, and the maximum radial cutoff is determined from the first minima occurring in $HB(r)$. Because neighbors are excluded based on the geometric criteria, the values of $HB(r)$ do not converge to 1 and the absolute values do not hold any significant meaning.

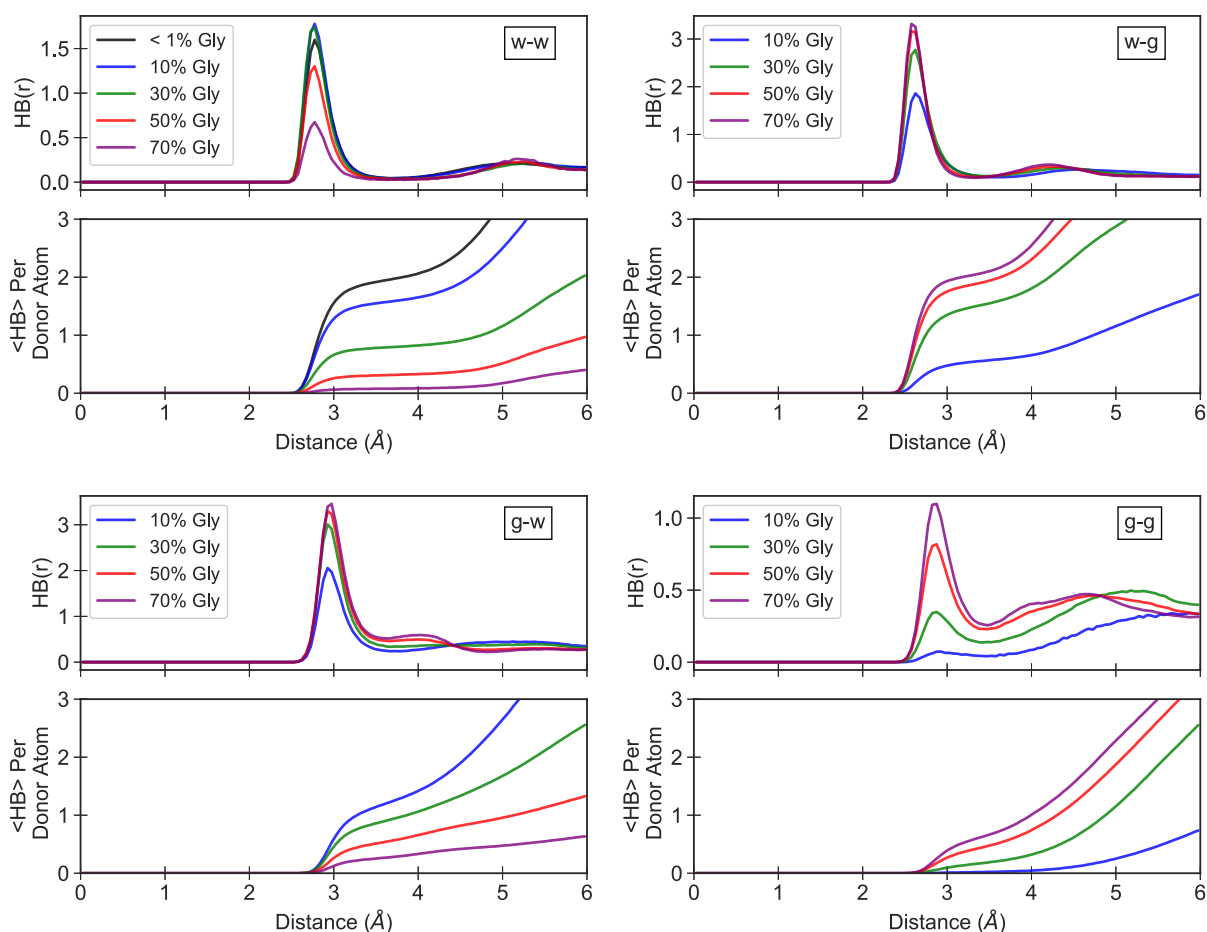


Figure 7. Modified RDF for donor-acceptor pairs that requires the neighbor to adhere to the H-bond angle criteria. Top plots show $HB(r)$ and plots below show the average number of H-bond pairs integrated from 0 to r .

When the angle criteria are imposed in the RDF's between donor-acceptor pairs, the distance of the minimum after the first peak becomes more consistent across different glycerol concentrations compared to the normal RDF's in Figure 5. In Figure 7, the minimum of $HB(r)$ after the first peak for w-w and w-g approaches close to 0 indicating a clear division between H-bonded neighbors in the first solvation shell and non H-bonded neighbors in the second solvation shell. This makes the calculation for the average number of H-bonds that a water oxygen is donating in, $\langle HB \rangle_w$, consistent for an assigned H-bond cutoff distance of 3.2 Å to 3.7 Å for the glycerol concentrations studied.

The minima after the first peak in g-g and g-w still contain a finite number of neighbors. Physically, this indicates that the maximum H-bond distance is less defined when glycerol oxygen acts as the donator. As a result, the value of $\langle HB \rangle_g$ becomes more dependent on the exact value assigned to the maximum H-bond cutoff radius. The maxima of the first peaks in the w-g and g-w $HB(r)$ each correspond to one of the peaks in the double-peak observed in the O_g-O_w and O_w-O_g RDF's in Figure 5. As previously indicated, the distance that O_w and O_g are separated by depends on which oxygen acts as a hydrogen donor. When O_w has a hydrogen oriented towards O_g , then the peak occurs around 2.7 Å. When O_g has its hydrogen oriented towards O_w , the peak occurs at 2.95 Å. For all H-bond definitions, the maximum radial cutoff for a H-bond is based on the minimum after the first peak of each $HB(r)$ at different concentrations of glycerol. The geometric criteria to define H-bonds in the system along with the average number of H-bonds per donor and acceptor atom are provided in Table 2.

Table 2. Hydrogen bond definitions for different donor-acceptor (d-a) oxygen pairs and for different concentrations of glycerol. The average number of a H-bond type per donor atom $\langle HB \rangle_d$ and acceptor atom $\langle HB \rangle_a$ is also provided.

w-w					
mol% glycerol	< 1	10	30	50	70
r (Å)	< 3.70	< 3.75	< 3.80	< 3.75	< 3.85
θ (deg)	< 35	< 35	< 35	< 35	< 35
$\langle HB \rangle_w$	1.96	1.59	0.80	0.32	0.08
$\langle HB \rangle_w$	1.96	1.59	0.80	0.32	0.08

w-g					
mol% glycerol	< 1	10	30	50	70
r (Å)	n/c	< 3.60	< 3.55	< 3.45	< 3.35
θ (deg)	n/c	< 35	< 35	< 35	< 35
<HB> _w	n/c	0.58	1.56	1.91	2.04
<HB> _g	n/c	1.75	1.21	0.64	0.29

g-w					
mol% glycerol	< 1	10	30	50	70
r (Å)	n/c	< 3.70	< 3.70	< 3.70	< 3.70
θ (deg)	n/c	< 50	< 50	< 50	< 50
<HB> _g	n/c	1.23	0.93	0.57	0.28
<HB> _w	n/c	0.41	1.19	1.67	1.94

g-g					
mol% glycerol	< 1	10	30	50	70
r (Å)	n/c	< 3.50	< 3.45	< 3.50	< 3.50
θ (deg)	n/c	< 50	< 50	< 50	< 50
<HB> _g	n/c	0.02	0.18	0.47	0.65
<HB> _g	n/c	0.02	0.18	0.47	0.65

3.5. Probability model for the Number of H-bonds in a Water-Glycerol System

By taking the average number for each type of H-bond per donor atom and determining the total number of H-bonds in a system, then the fraction of each type of H-bond at each concentration of glycerol can be obtained. From Figure 8, the fraction of H-bonds between glycerol and water molecules, w-g and g-w, reaches a maximum for the 30 mol% glycerol system. However, because there is no way to determine the error in the calculated values of <HB> compared to the “true” values of <HB>, and thus the reliability of the trend, a reasonable model is supplied to justify the trends based on the probability of randomly assigning H-bond pairs.

To calculate the fraction of a given type of H-bond in a system based on equally favored conformations, the number of ways that one specific donor-acceptor pair can form in a system is

compared to the total number of donor-acceptor pairs that can form. In a water-glycerol system containing N molecules and a glycerol molar fraction of C , then the total number of water oxygen atoms, n_w , and glycerol oxygen atoms, n_g are:

$$n_w = N * (1 - C) \quad (10)$$

$$n_g = N * 3C \quad (11)$$

For the 4 different types of intermolecular H-bonds in the system, w-w, w-g, g-w, and g-g, the number of possible conformations of each donor-acceptor pair, P_{da} , is:

$$P_{ww} = n_w * (n_w - 1) \quad (12)$$

$$P_{wg} = n_w * n_g \quad (13)$$

$$P_{gw} = n_g * n_w \quad (14)$$

$$P_{gg} = n_g * (n_g - 3) \quad (15)$$

The total number of possible hydrogen bonds that water can act as a donor in is the sum of P_{ww} and P_{wg} . Then, the fraction of w-w H-bonds compared to the total number of H-bonds that water oxygen is acting as a donor in is:

$$\%W_{ww} = \frac{P_{ww}}{P_{ww} + P_{wg}} \quad (16)$$

The remainder of the fractions are similarly obtained:

$$\%W_{wg} = \frac{P_{wg}}{P_{ww} + P_{wg}} \quad (17)$$

$$\%G_{gg} = \frac{P_{gg}}{P_{gg} + P_{gw}} \quad (18)$$

$$\%G_{gw} = \frac{P_{gw}}{P_{gg} + P_{gw}} \quad (19)$$

Now, the total number of each H-bond in the system, N_{da} , can be determined by taking the fraction of each H-bond conformation per donor atom and multiplying by the number of donor atoms in

the system. An additional multiplying factor is added on to account for each water oxygen donating in 2 H-bonds simultaneously and glycerol usually donating in 1 H-bond.

$$N_{ww} = \%W_{ww} * n_w * 2 \quad (20)$$

$$N_{wg} = \%W_{wg} * n_w * 2 \quad (21)$$

$$N_{gg} = \%W_{gg} * n_g * 1 \quad (22)$$

$$N_{gw} = \%W_{gw} * n_g * 1 \quad (23)$$

The final fraction of each H-bond in the system is then determined by taking N_{da} and dividing by the total number of H-bonds in the system.

A second model is considered to account for the interdependence of possible H-bonds involving glycerol oxygen. Because there are three glycerol oxygen that are closely associated by a carbon backbone, assigning one possible H-bond to one of the glycerol oxygen may influence the possible H-bonds that the other two intramolecular glycerol oxygen can form. A way to approximate the dependence of the three intramolecular glycerol oxygen on each other is by determining the number of possible conformations based on the number of glycerol molecules rather than the number of glycerol oxygen. This modifies the possible conformations of H-bonds, P_{da} , to be:

$$P_{ww} = n_w * (n_w - 1) \quad (24)$$

$$P_{wg} = n_w * \left(\frac{n_g}{3}\right) \quad (25)$$

$$P_{gw} = n_g * n_w \quad (26)$$

$$P_{gg} = \frac{n_g}{3} * \left(\frac{n_g - 3}{3}\right) \quad (27)$$

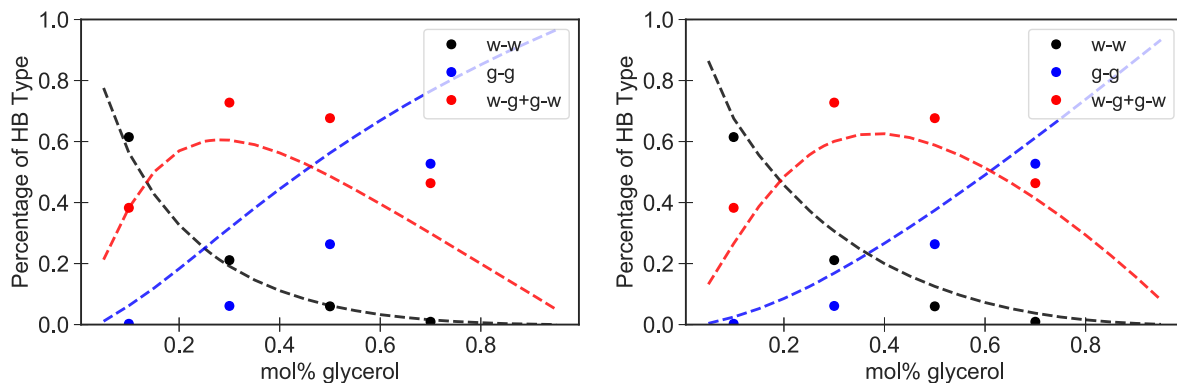


Figure 8. Fraction of w-w, w-g, g-w, and g-g H-bonds as a function of glycerol concentration. Values obtained from simulations are shown as points. Dotted lines are the values obtained from the probability model to predict the fraction of the H-bond of the corresponding color. MD results plotted against the probability model using the number of glycerol atoms (Left) and the number of glycerol molecules (Right).

Based on the comparison of the two probability models in Figure 8, the model that assumes an interdependence of the possible H-bonds that form for intramolecular glycerol oxygen more closely fits the results from MD simulations. Both models predict the contribution of w-w H-bonds reasonably well, but the inflection of the trend for the fraction of g-g H-bonds is more closely modeled by an interdependence of intramolecular glycerol oxygen. However, both models consistently underestimate the contributions of w-g and g-w H-bonds as well as overestimate g-g contributions compared to the MD results. This could either be due to oxygen having a preference to H-bond to opposite molecules or an overestimation of w-g and g-w H-bonds based on the H-bond criterion used. From static analysis alone, it is difficult to determine if the observed fractions of HB types are due to purely entropic effects or also an increased affinity for creating H-bonds with opposite molecules. For this reason, the dynamics of the H-bonds in water-glycerol systems are also analyzed to determine if there is a non-equal preference for one H-bond type over another.

3.6. Hydrogen Bond Dynamics

3.6.1. Measuring Hydrogen Bond Dynamics in Molecular Simulations

Previous work has used many different methods to extract the underlying dynamic parameters for HB's. However, almost all hydrogen bond dynamic studies use a form of a hydrogen bond

autocorrelation function (HBACF) [37, 28, 27, 38, 39, 40, 41, 29]. The basic HBACF, $c(t)$, determines the fraction of the hydrogen bonds present at $t=0$ that also exist at a given time t . By fitting a rate expression to the relaxation of the initial population of hydrogen bonds, a rate of hydrogen bond breaking can be extrapolated. Previous research on H-bond dynamics have indicated that autocorrelations follow a near-exponential decay which suggests a first-order kinetics process [27, 38, 40]. If the only process influencing the relaxation of the initial H-bond population is the rate of H-bond breaking, then the rate of relaxation follows:

$$\frac{dc(t)}{dt} = -k_b c(t) \quad (28)$$

with k_b being the rate of H-bond breaking. However, the deviations in HBACF's from purely exponential decay suggest additional phenomena affect the relaxation of the initial H-bond population. The deviation from exponential decay has been identified to be the ambiguity of when hydrogen bonds terminate [38]. Hydrogen bonds contain librational motions that will cause the geometric criteria to be temporarily violated throughout the lifetime of a hydrogen bond. When a H-Bond terminates, the distance between two oxygen atoms can cross an arbitrary distance cutoff several times before completely moving from the first solvation shell to the second (See Fig. 3 from ref. [37]). Some groups attempt to mask the "false breaking" effects by allowing HB's to violate the criteria for less than a critical violation time, t^* [29, 40, 39].

HB's also have a chance to reform after some period of time after rupturing. This would mean that the H-bond population existing at time t could contain previously broken and reformed H-bonds. Thus, continuous H-Bond autocorrelation functions are also calculated to prevent the diffusion and reformation of H-bonds from affecting the correlation [28, 41, 37].

The difficulty in assessing hydrogen bond dynamics is accounting for "false breaking" that occurs on short timescales and also reformation on long timescales. Allowing hydrogen bonds to violate the bonding criteria for a period of time requires the assignment of an arbitrary critical violation time, t^* . Increasing t^* increases the effects of diffusion on the relaxation of the hydrogen bond population. On the other end, using a continuous H-Bond autocorrelation function captures both the true rate of H-Bond breaking as well as the rate of librational motions corresponding to "false breaking" [38].

A. Luzar had summarized that changing the geometric criteria, arbitrary violation allowance time, and sampling frequency will have an effect on the measured H-bond dynamic parameters for most methodologies that attempt to compensate for diffusion or false breaking [38].

This conclusion bodes badly for trying to compare H-bond dynamics between different types of H-bonds because the different parameters obtained may not be due to the fundamental behavior of the H-bonds but rather due to the arbitrary criteria, like the different H-bond definitions, employed.

However, a reactive flux network approach with a combined kinetic-diffusive model of hydrogen bond breaking and reformation was developed that allowed for the kinetic parameters of H-bonding to be separated from the influences of diffusion [27]. More importantly, the approach allows the kinetic parameters of different H-bonds to be compared without having the geometric criteria or any arbitrary violation parameter affect the measured dynamic parameters. Using this approach allows for the dynamic properties of the different H-bonds in water-glycerol solutions to be quantitatively compared and ultimately identify if there is a non-equal preference to form one type of H-bond over another. The remainder of this subchapter describes the implementation of the kinetic-diffusive model developed in ref. [27].

To account for diffusion in the relaxation of an initial H-bond population, H-bond reformation is included in the kinetic rate equation. Any H-bond pairs that are no longer H-bonded, but still in close proximity to each other, at time t are considered to be part of a non-bonded neighboring population, $n(t)$. Former H-bond pairs within $n(t)$ are assumed to have a first-order rate of conversion back into the H-bond population, $c(t)$.

$$\frac{dc(t)}{dt} = -k_b c(t) + k_r n(t) \quad (29)$$

where k_r is the rate constant for H-bond reformation from former H-bond pairs in $n(t)$. The former H-bond pairs within $n(t)$, in addition to reforming, can also diffuse away from each other and be separated far enough that H-bond reformation is not immediately possible. The effects of diffusion on $n(t)$ is modeled by Fickian diffusion. The rate of change in $n(t)$ is a combination of Fickian diffusion over the entire space domain and the conversion of H-bond pairs between $c(t)$ and $n(t)$ occurring within a volume a^3 with “ a ” being the range of lengths a hydrogen bond could exist.

$$\frac{d}{dt}\rho(r,t) = D\nabla^2\rho(r,t) + \delta(r)[k_b c(t) - k_r n(t)] \quad (30)$$

where $\rho(r,t)$ is the density of the unbonded pairs with a radius r corresponding to the distance outside of the range where H-bond pairs can convert between $c(t)$ and $n(t)$, and D is the diffusion coefficient between the specific H-bond pair. With this definition of r , the interconversion between $c(t)$ and $n(t)$ only occurs within $r=0$. Additionally, the value of $\rho(0,t)$ is

$$\rho(0,t) = \frac{n(t)}{a^3} \quad (31)$$

Solving for the governing equations for $c(t)$ and $n(t)$ simultaneously results in the following equation for the rate of change of the H-bond population in the Laplace domain

$$-\frac{dC(s)}{ds} = \frac{k_b}{s + k_b + k_r s F(s)} \quad (32)$$

where $F(s)$ is

$$F(s) = 3\tau_d [1 - \sqrt{s\tau_d} \arctan\left(\frac{1}{\sqrt{s\tau_d}}\right)] \quad (33)$$

The additional term τ_d corresponds to the diffusion coefficient and “a” by:

$$\tau_d = \frac{a^2}{D(6\pi^2)^{2/3}} \quad (34)$$

In the study that developed the reactive flux model [27], appropriate values of k_b and k_f were determined by a numerical fit by using the measured values of $c(t)$ and $n(t)$ from simulations and plotted against the measured $\frac{dc(t)}{dt}$ according to the rate $k_r n(t)$ in equation (29). The value of τ_d was determined by fitting the inverse Laplace transform of equation (32) against the measured $\frac{dc(t)}{dt}$ using the same values of k_b and k_f determined previously.

The approach allowed identical rates of H-bond breaking, k_b , to be determined for both loose and strict HB criteria [38]. The reactive flux network, combined with a rate expression for H-bond breaking and reformation, was able to incorporate the effects that diffusion has on the autocorrelation function of the initial H-bond population. By using the above approach to analyze the H-bonds in water-glycerol systems, the kinetic parameters obtained for the different H-bonds are independent of the geometric criteria used and can be quantitatively compared.

3.7.2. Accounting for the Transient Period in H-bond Autocorrelation Functions with an Adjusted $c(0)$

The above reactive flux approach proposed by Luzar et al. is also used in this study. However, a different approach is used to normalize the H-bond dynamics between different models. In order for the effects of different H-bond criteria to be neglected in the previous study, the measured rate of change had to be determined by the initial rate of H-bond breaking at $t=0$, k_{TST} , and a time dependent dynamical transmission coefficient, $\kappa(t)$,

$$k(t) = \kappa(t) \times k_{TST} \quad (35)$$

The reasoning for this modification comes from the “false breaking” of H-bonds as a result of the arbitrary geometric criteria used to identify H-bonds. Different geometric criteria will identify

different fractions of the total “true” H-bond population at a given instant. From the initial H-bond population identified at $t=0$, there is a transient period where the H-bond population relaxes to occupy the other possible conformations of a H-bond. In this transient period, the rate of decrease of $c(t)$ is influenced by fast vibrational fluctuations of H-bonds in addition to genuine H-bond breaking and formation. An example of the transient period is shown in Figure 9. provide an example on normalizing the observed rate based on the geometric criteria, imagine the relaxation of an initial H-bond population identified by strict and lenient geometric criteria. Of the “true” H-bonds existing at $t=0$, the strict criteria will identify fewer H-bonds than the lenient criteria, but the measured $c(0)$ using both H-bond criteria is, by definition, 1. The H-bonds identified by the two criterion at $t=0$ will undergo fast liberational motions and will relax to occupy the other legitimate geometric conformations of H-bonds during an initial transient period. The strict geometric definition measures fewer possible conformations of H-bonds than the lenient criteria, so at time t after the transient period, the value of $c(t)$ will be smaller using the strict criteria than the measured $c(t)$ using the lenient criteria. After the transient period, only the true H-bond dynamics will influence the rate of change of $c(t)$. Because the values of $c(t)$ are different due to the transient period, the observed rates, which are dependent on the value of $c(t)$, will also be different. The dynamical transmission coefficient calculated in the work by Luzar et al. accounts for these differences by effectively determining what the initial population, $c(0)$, measured by each geometric criteria would be if the effects of the transient period were excluded [38].

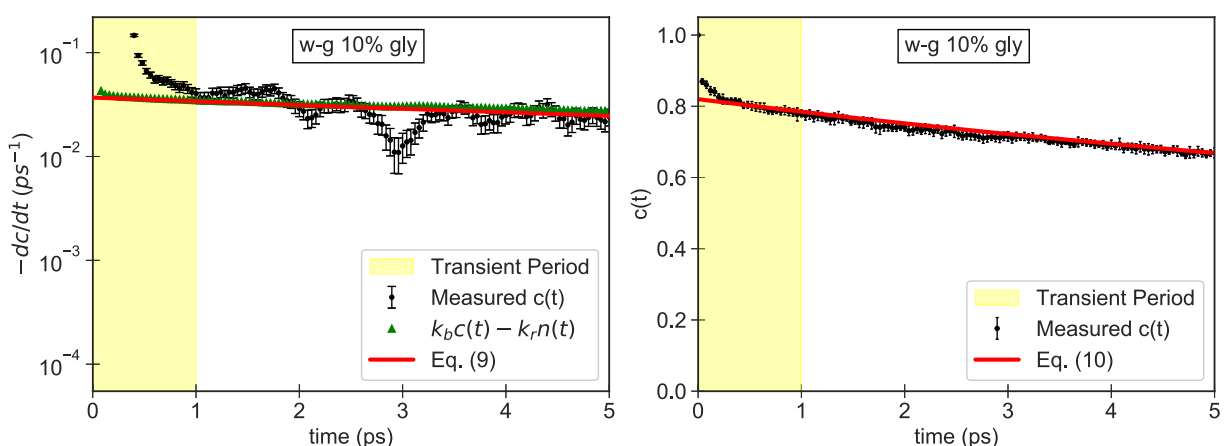


Figure 9. Initial relaxation of a *w-g* H-bond population in a 10 mol% glycerol system. The transient period is highlighted in yellow where the initial H-bond population relaxes to other H-

bond conformations not allowed by the geometric criteria and “false” H-Bonds rapidly disassociate. The rate of change in the H-bond correlation is calculated from equation (29) and measured values of $c(t)$ and $n(t)$, and the models in equations (36) and (37) are fit to the measured values of $c(t)$ using $k_b = 0.045\text{ps}^{-1}$, $k_r = 0.04\text{ps}^{-1}$, $\tau_d = 16\text{ps}$, and $c(0) = 0.82$. Error bars are 95% confidence intervals.

In this work, the initial H-bond population at $c(0)$ is estimated from extrapolation of the behavior after the transient period rather than using the dynamical transmission coefficient. The reasoning is that, as explained in ref. [38], to get an accurate measurement of k_{TST} and $\kappa(t)$, the number of H-bonds changing between $c(t)$ and $n(t)$ had to be calculated every timestep (every 1fs) or $k(t)$ would be underestimated due to “hot” trajectories. In this work, H-bonds are calculated post-simulation. While this offers flexibility for running new analysis on MD trajectories post-stimulation, it requires exporting the coordinates for every timestep that will be analyzed post-simulation. If the number of H-bonds converting between $c(t)$ and $n(t)$ were calculated every timestep, then very large file sizes would need to be generated in order to calculate the dynamical transmission coefficient over a long period of time. To reduce the file size, the coordinates are exported less frequently, ranging from 10 fs to 20 ps, depending on how fast the dynamics of a particular H-bond is. It should be noted that the sampling frequency will not affect the measured $c(t)$ or $n(t)$ for a given timestep as these are history independent, but it will affect the observed number of individual H-bonds interconverting over a given period of time. For this reason, neither $\kappa(t)$ nor k_{TST} can be accurately calculated with larger timesteps between trajectories, so an alternative approach is used to compensate for the transient period based on extrapolating $c(0)$.

The initial values of $c(0)$ are then incorporated into the kinetic-diffusion model proposed by Luzar et al. When initially solved, the assumption is that $c(0)$ must be 1 and $n(0)$ is 0, but when introducing the possibility of a different $c(0)$, the rate of change in the H-bond population is modeled by:

$$-\frac{dC(s)}{ds} = \frac{k_b c(0)}{s + k_b + k_r s F(s)} \quad (36)$$

Correspondingly, the value of the H-bonded population in the Laplace domain is given by:

$$C(s) = \frac{-k_b c(0)}{s[s + k_b + k_r s F(s)]} + \frac{c(0)}{s} \quad (37)$$

The values of $c(t)$ and its derivative in the time domain can be determined by a numerical inverse Laplace transform (details in the Appendix).

3.7.3. Data Collection and Error Analysis for H-bond Dynamics

All dynamic H-bond analysis performed are based off of averages of 8 trials with different starting H-bond populations. Different time intervals are used to examine the relaxation of $c(t)$ depending on how long it takes to see a significant decay in $c(t)$ for a given H-bond type and concentration. These intervals range from 20 ps to 5 ns. Over the specified interval, atomic trajectories are exported over 500 evenly spaced timesteps to determine $c(t)$, $n(t)$, and $\frac{dc(t)}{dt}$. Data smoothing is performed on the measured values of $\frac{dc(t)}{dt}$ by taking the average slope of $\frac{dc(t)}{dt}$ and the 8 successive and 8 previous values of $\frac{dc(t)}{dt}$. Error bars shown, unless otherwise specified, are based off of 95% confidence intervals assuming that the 8 trials adhere to a Student's t-distribution.

The initial values of k_b and k_r are determined by fitting equation (29) to the measured $\frac{dc(t)}{dt}$, $c(t)$, and $n(t)$. Afterwards, the initial values of k_b and k_r are refined by fitting equation (37) to the measured values of $c(t)$ as well as determining the value for τ_d . The measured values of $c(t)$ have less relative uncertainty than the values of $\frac{dc(t)}{dt}$, so the kinetic and diffusive parameters can be assigned more precisely by fitting to $c(t)$.

3.7.4. Properly Assigning Values to the Kinetic and Diffusive Terms in the H-Bond Autocorrelation Model

Admittedly, the transient period is difficult to locate without first identifying the kinetic model parameters that fit to a majority of the relaxation of $c(t)$. If the model is not fit to a long enough period of time to observe a significant decay in $c(t)$, then the rate parameters obtained could be overestimated.

An example of improperly fit parameters for the kinetic-diffusive model of $c(t)$ is provided in Figure 10. An initial set of kinetic parameters were assigned to the model by only looking at the relaxation of $c(t)$ for w-g H-bonds in 10 mol% glycerol over an interval of 20 ps. The parameters are referred to as the "Early Fit Model" because the parameters assigned only predict the values of $c(t)$ at early stages in the relaxation of $c(t)$. Note that after 20 ps, half of the original H-bond

population (adjusted for the transient period) still persists. After the “Early Fit Model” was created, the relaxation of the H-bond population was analyzed over a longer interval of time of 500 ps. Over this period of time, almost all w-g H-bonds that are detected at $t=0$ terminate. The new parameters assigned in the “Full Fit Model” are able to predict the value of $c(t)$ from the initial relaxation to the time where most of the H-bond population terminates. One of the differences between the models is the value assigned to the rate of H-bond breaking, k_b . The “Early Fit Model” has a larger k_b because a portion of the transient period occurring from 0.5-1.0 ps influences the fit of the kinetic model. During the transient period, the rate of H-bond population decay is larger, so a higher value of k_b is fit to the data. The “Full Fit Model” only has measurements of $c(t)$ and $n(t)$ every 1 ps, so most of the transient period is excluded from the data used to fit the “Full Fit Model”. From previous research, the transient period of the pure water model studied was around 0.2 ps [38], but in this study, the transient period is found to be as long as 10 ps for high concentrations of glycerol. This longer transient period may mean that processes other than vibrational motions are occurring during the transient period. Some additional part of the transient period could be false positive H-bonds. From the modified RDF in Figure 7, the non-zero value of $HB(r)$ at the radial cutoff for g-w and g-g H-bonds indicates an intersection between the H-bonded population in the first peak and the second solvation shell in the second peak. At time 0, some of the H-bonds identified could be neighbors primarily residing in the second solvation shell, but due to vibrational motions, temporarily ended up within the criteria for an H-bond. This may contribute to the longer transient periods observed in glycerol-water solutions.

The demonstration in Figure 10 shows the importance of measuring the relaxation of $c(t)$ for a long enough period of time to ensure that the parameters corresponding to H-bond reformation, k_b and τ_d , predict the relaxation of $c(t)$ at longer times.

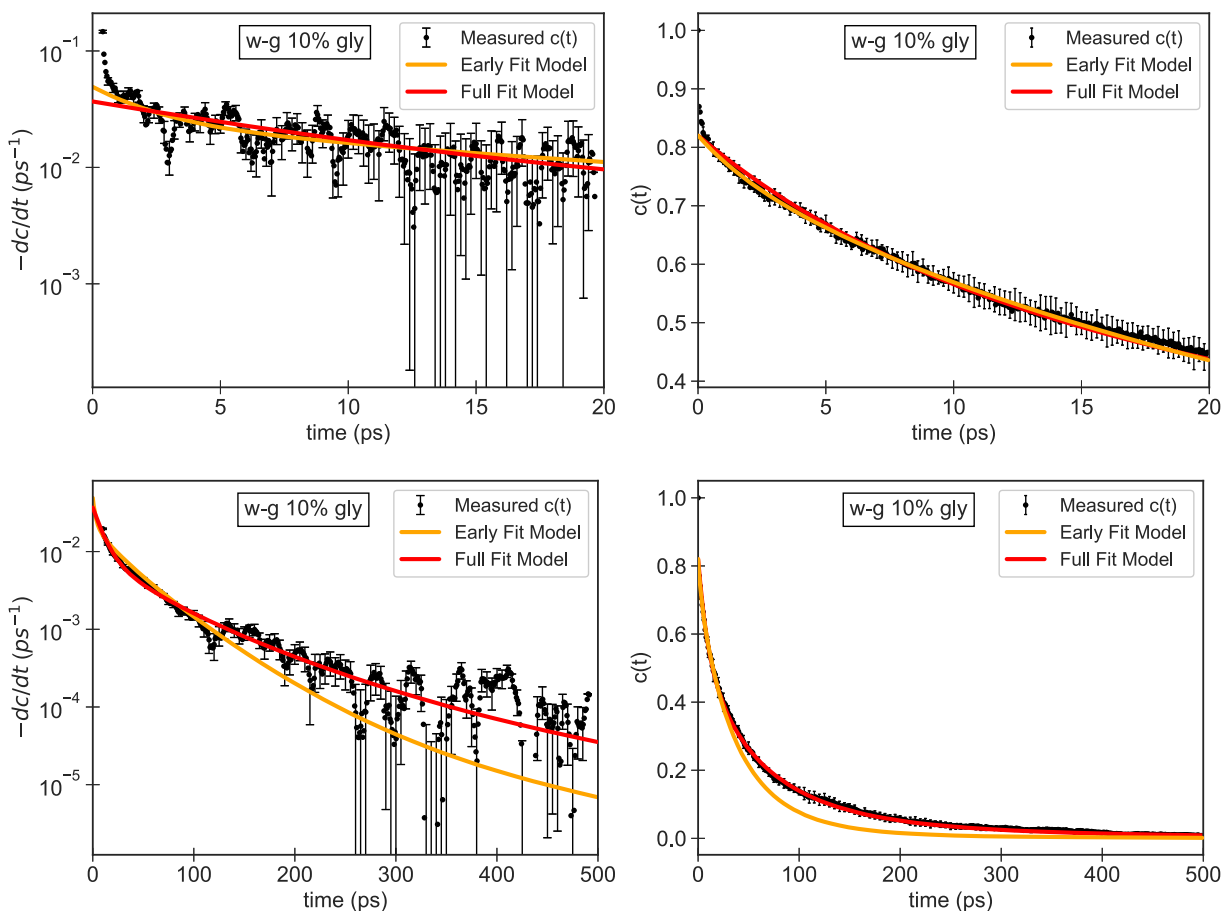


Figure 10. Demonstration of improperly fitting the H-bond kinetic-diffusive parameters in equations (36) and (37) if fit to too small of a time interval. The “Early Fit Model” uses the parameters $k_b = 0.06\text{ps}^{-1}$, $k_r = 0.2\text{ps}^{-1}$, $\tau_d = 2.5\text{ps}$, and $c(0) = 0.82$ fit over 20ps of relaxation. The “Full Fit Model” uses the parameters $k_b = 0.045\text{ps}^{-1}$, $k_r = 0.04\text{ps}^{-1}$, $\tau_d = 16\text{ps}$, and $c(0) = 0.82$ fit over 500ps of relaxation.

3.7.5. Adjusting the measured non-bonded proximity H-bond Population, $n(t)$

The measured non-bonded pair population $n(t)$ must also be compensated for the transient period. Similar to how $c(t)$ will decay more quickly during the transient period, the population of $n(t)$ will quickly increase during the transient period due to fast vibrational motions. Some of the H-bond pairs transitioning from $c(t)$ to $n(t)$ are due to genuine H-bond breaking, but many of the pairs initially observed to be in $n(t)$ are due to the relaxation of the initial H-bond population into conformations of an H-bond that are not allowed by a specific geometric criteria. While the

geometric criteria will consider both types of pairs as part of $n(t)$, the H-bonds that are still “truly” H-bonded but outside the geometric criteria should be excluded from the population of $n(t)$. According to the kinetic rate equation used, $n(t)$ consists of close but unbonded pairs of H-bonds that were detected at $t=0$ that can transition back into the bonded population, $c(t)$, through reformation. Because some of the pairs in $n(t)$ are unaccounted H-bonds, the measured value of $n(t)$ will overestimate the population of unbonded pairs that can convert back into the bonded population through the rate of H-bond reformation, k_r .

Ideally, the true population of close non-bonded pairs, $n_{true}(t)$, would like to be known by excluding the “truly H-bonded i.e. falsely not H-bonded” pairs found in $n(t)$ at any given time, $n_{false}(t)$. By using the rate of change of $n(t)$ after the transient period to extrapolate a value of $n(0)$, similar to how $c(0)$ is obtained, the fraction of the initial H-bond population that are “true” H-bond pairs but detected within $n(t)$ can be calculated.

The effect of calculating $n(0)$ and $c(0)$ is determining the equilibrium values of the H-bond population within $c(t)$ and $n(t)$ due to fast vibrational motions and specific geometric criteria of H-bonds employed before any genuine H-bond breaking occurs. The transient period can be thought of as the interval where equilibrium is rapidly established between the detected H-bonds in $c(t)$ and the “true” H-bonds that are not accounted for by the geometric criteria, $n_{false}(t)$. During the transient period, the rate of change of $c(t)$ would more realistically follow:

$$\frac{dc(t)}{dt} = -k_b c(t) + k_r n_{true}(t) + [-f_1(c(t)) + f_2(n_{false}(t))] \quad (38)$$

Where f_1 and f_2 are arbitrary functions of $c(t)$ and $n_{false}(t)$ that describe fast vibrational motions that cause H-bonds to rapidly interconvert between $c(t)$ and $n_{false}(t)$. However, once equilibrium is established between the populations of $c(t)$ and $n_{false}(t)$, then the transient terms in the brackets cancel each other out and the rate equation becomes identical to eqn. (29). Once equilibrium is established, then the transient period ceases and the rate of $c(t)$ will only be controlled by H-bond dynamics and diffusion. After the transient period, equilibrium between $c(t)$ and $n_{false}(t)$ indicates:

$$\frac{n_{false}(t)}{c(t)} = const. \quad (39)$$

Where the constant can be determined by the extrapolated values of $n(0)$ and $c(0)$. This allows for the value of $n_{true}(t)$ to be calculated for any time after the transient period

$$n_{true}(t) = n(t) - n_{false}(t) = n(t) - \frac{n(0)}{c(0)} c(t) \quad (40)$$

Realistically, some “true” H-bonds may lie outside both criteria to be detected in either $c(t)$ or $n(t)$. However, as long as a sufficiently large cutoff radius for H-bonds is specified, most “true” H-bonds will exist in either the $c(t)$ or $n(t)$ population at any given time. Even with the adjustment for $n_{\text{true}}(t)$, correlating $\frac{dc(t)}{dt}$, $c(t)$, and $n(t)$ to the rate model in equation (29) only works at times near the beginning of the H-bond population relaxation.

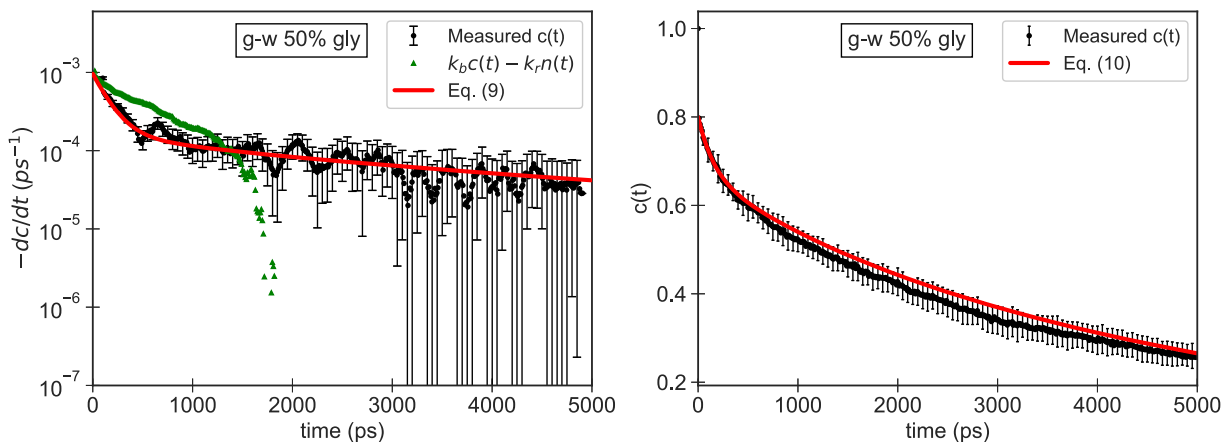


Figure 11. Relaxation of *g-w* H-bonds in a 50 mol% glycerol system. The model is the inverse Laplace transform of equation (37) with the fitted parameters $k_b = 0.0012$, $k_r = 0.0042$, $\tau_d = 480\text{ps}$, and $c(0) = 0.80$.

At long times, the predicted rate of H-bond decay using equation (29) is much lower than the actual change in the H-bond population. The reason for the model failing at longer times is most likely due to only a subset of $n_{\text{true}}(t)$ being able to transition back into $c(t)$ at any given time. However, the values of k_b and k_r fit to the kinetic rate model at early times can be used as initial guesses for the models of $-\frac{dc(t)}{dt}$ and $c(t)$ in equations (36) and (37), respectively.

Even though the kinetic model that equations (36) and (37) are based off of cannot predict the decay of $c(t)$ at longer times, equations are still able to predict $c(t)$. This suggests that the fundamental principle of H-bond breaking, and reformation combined with diffusion is still a good model for $c(t)$. Presently, the current method used to measure $n(t)$ needs refining in order for equation (29) to predict the decay in $c(t)$. This may require knowing more information about the former H-bond pairs in $n(t)$ such as the other H-bonds that they are participating in.

3.7.6. Independence of H-bond Kinetic and Diffusive Parameters from H-bond Criteria

In order to support that the modified approaches to analyzing the dynamic properties of H-bonds are still independent of the specific H-bond criteria used, the relaxation of g-g H-bonds in 70 mol% glycerol concentration is studied with two different H-bond criteria. The first H-bond criteria is the one specified in Table 2. The second H-bond criteria uses a larger cutoff radius of 4.05 Å and a different angle criterion. Instead of having the oxygen donor atom acting as the root of the angle, the hydrogen atom acts as the root of the angle between the donor and acceptor atom. With this definition, the closer the angle is to 180°, the more linear the H-bond is. A minimum angle cutoff is specified at 150°. This angle criterion is somewhat more restrictive than the former angle specified.

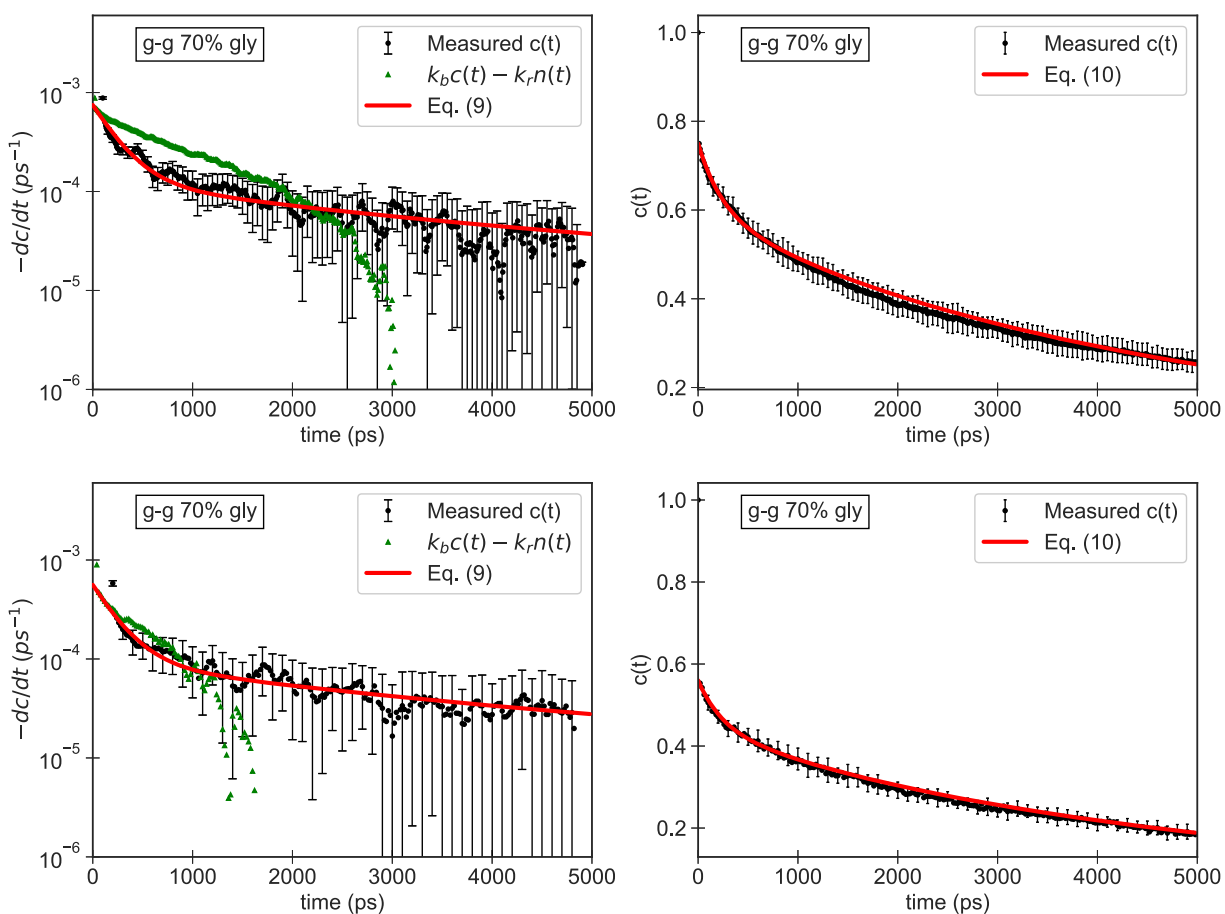


Figure 12. Relaxation of g-g H-bonds in a 70 mol% glycerol system measured using two different H-bond criteria. Equation (37) models the relaxation of both H-bond populations with different H-bond criteria with the same dynamic and diffusive parameters of $k_b = 0.001$, $k_r = 0.0025$, and $\tau_d = 700$ ps. The only difference in the models is the initial value of $c(0)$. For the original H-bond

criteria (Top), the value of $c(0)$ is 0.75. For the alternative H-bond definition (Bottom), the value of $c(0)$ is 0.56.

The relaxation of a H-bond population using the two different geometric criteria is compared in Figure 12. Using the same kinetic and diffusive parameters for equations (36) and (37), the decay of both H-bond populations are predicted despite having different values of $c(t)$. Because the two geometric criteria measure different amounts of the “true” H-bond population, the transient period causes the extrapolated values of $c(0)$ to be different. The model with a larger cutoff radius and a stricter angle criteria accounts for a smaller subset of the “true” H-bond population as indicated by the smaller value of $c(0)$. It may also be possible that the larger cutoff radius for the second geometric criteria incorporates “false” H-bonds at $t=0$ that quickly decay from the measured H-bond population and also reduce $c(0)$.

Based on the ability for the model of $c(t)$ given by equation (37) to predict the measured values of $c(t)$ for both H-bond criteria, it gives some confidence that extrapolating the value of $c(0)$ is a suitable alternative to using the dynamical transmission coefficient used in the study that initially utilized the combined kinetic-diffusive model for the relaxation of an initial H-bond population.

w-w					
mol% glycerol	< 1	10	30	50	70
k_b (ps⁻¹)	0.28 ± 0.03	0.118 ± 0.002	0.0046 ± 0.0008	0.0030 ± 0.0009	n/c
k_r (ps⁻¹)	0.20 ± 0.12	0.034 ± 0.002	0.0018 ± 0.0009	0.0018 ± 0.0011	n/c
τ (ps)	1.0 ± 0.4	12 ± 2	397 ± 100	1021 ± 430	n/c

w-g					
------------	--	--	--	--	--

mol% glycerol	< 1	10	30	50	70
k_b (ps⁻¹)	n/c	0.045 ± 0.008	0.0028 ± 0.0005	0.0018 ± 0.0002	0.0013 ± 0.0003
k_r (ps⁻¹)	n/c	0.035 ± 0.015	0.0016 ± 0.0007	0.0017 ± 0.0005	0.0013 ± 0.0007
τ (ps)	n/c	19 ± 4	573 ± 160	1114 ± 322	1507 ± 818

g-w					
mol% glycerol	< 1	10	30	50	70
k_b (ps⁻¹)	n/c	0.065 ± 0.003	0.0025 ± 0.0007	0.0015 ± 0.0008	0.0012 ± 0.0005
k_r (ps⁻¹)	n/c	0.044 ± 0.005	0.0033 ± 0.0028	0.0058 ± 0.0064	0.0041 ± 0.0030
τ (ps)	n/c	12.7 ± 1	305 ± 156	492 ± 339	698 ± 362

g-g					
mol% glycerol	< 1	10	30	50	70
k_b (ps⁻¹)	n/c	n/c	0.0040 ± 0.0016	0.0018 ± 0.0010	0.0010 ± 0.0003
k_r (ps⁻¹)	n/c	n/c	0.0062 ± 0.0054	0.0077 ± 0.0080	0.0027 ± 0.0018
τ (ps)	n/c	n/c	223 ± 113	438 ± 342	773 ± 428

Table 3. Summary of the kinetic and diffusive parameters used to model $c(t)$ and its derivative based on equations (36) and (37). Values reported are averages and the error is the estimated

95% confidence interval. Averages and confidence intervals are obtained from a Monte-Carlo sensitivity analysis described in Appendix III.

The average values for k_b , k_r , and τ_d for different H-bonds at different concentrations of glycerol are provided in Table 3. Note that using the average values for all three parameters to fit the relaxation of $c(t)$ may not be the best fit. Instead, the confidence intervals specified for each parameter indicate that a majority of the measured values of $c(t)$ can be predicted if each of the three parameters are picked from within the confidence intervals specified. Once a value for one of the parameters is specified, then the range of possible values for the other two parameters will be further constrained.

In general, the relative uncertainty for k_b is less than the uncertainty in k_r and τ_d . This is because, in equation (37), k_r and τ_d appear as product pairs, so similar predicted values of $c(t)$ can be generated as long as the product of k_r and τ_d remain the same. From a physical standpoint, this means that the rate of H-bond reformation is difficult to decouple from the rate that former H-bond pairs diffuse away from each other. However, the value of k_b is somewhat less dependent on the selected values of k_r and τ_d , so the predicted values of $c(t)$ are more sensitive to changes in k_b .

The most important trend to note from Table 3 is that the rate of all H-bond dynamics decreases as the concentration of glycerol increases. Rates of H-bond breaking, H-bond reformation, and H-bond pair diffusion, which is inversely proportional to τ_d , all decrease with increasing glycerol concentrations. For the rate of H-bond breaking, k_b , in w-w H-bonds, the rate decreases the most between 10 mol% glycerol and 30 mol% glycerol solutions. At concentrations of 10 mol% glycerol or less, w-w H-bond breaking is $O(0.1)$ ps⁻¹ as opposed to $O(0.001)$ ps⁻¹ for glycerol concentrations of 30 mol% or higher. A similar order of magnitude change in H-bond dynamics occurs for the other types of H-bonds between 10 mol% and 30 mol% glycerol as well.

Compared to the dynamic H-bond parameters obtained for the SPC water model used in ref. [27], the TIP4P/2005 water model has slightly slower H-bond dynamics. The slower dynamics of TIP4P/2005 water are estimated to agree with the experimental relaxation time correlated to H-bond dynamics obtained from coherent QENS more closely than the SPC water model [7].

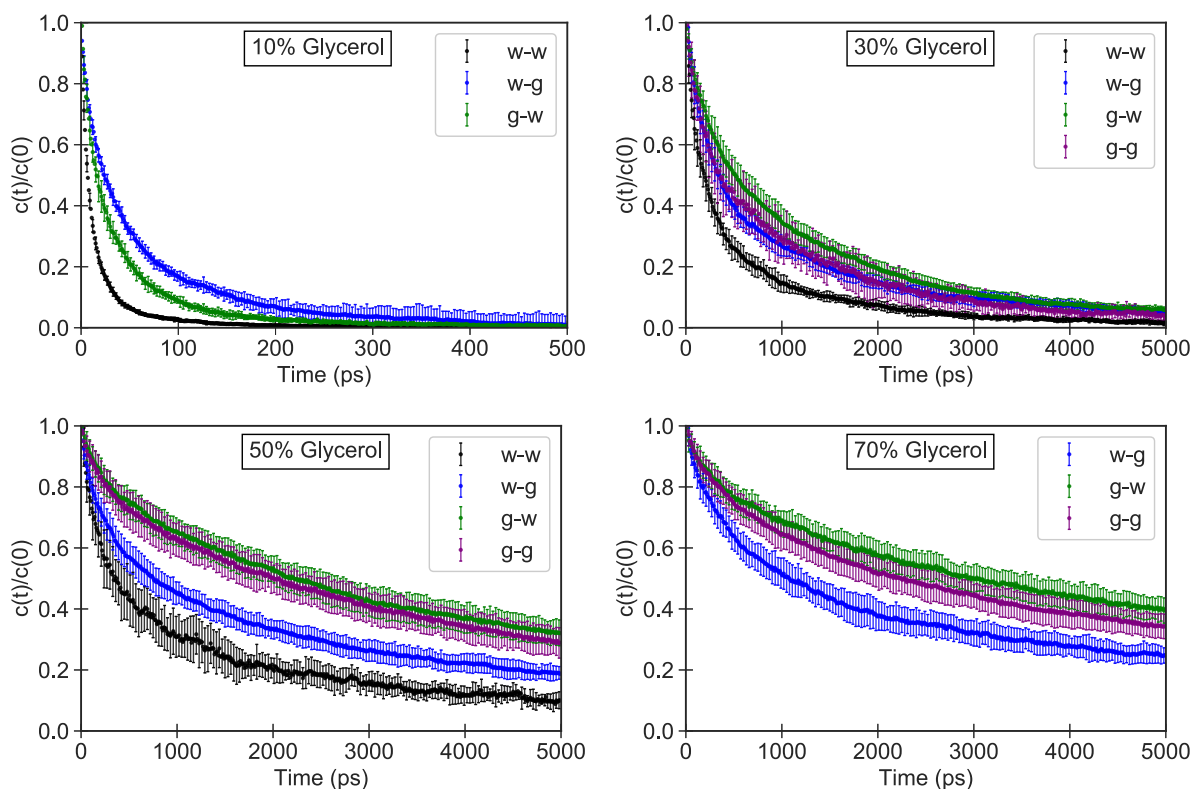


Figure 13. Comparison of H-bond correlation times normalized to the initial H-bond population accounting for the transient period, $c(0)$. (Top left) 10 mol% glycerol (Top right) 30 mol% glycerol (Bottom left) 50 mol% glycerol (Bottom right) 70 mol% glycerol. Error bars represent the standard deviation for $c(t)/c(0)$ accounting for an estimated standard deviation of ± 0.02 for estimating $c(0)$.

3.7.7. Identifying Non-Equal Preference for H-Bonds using Dynamic H-Bond Analysis

Beyond identifying kinetic and diffusive parameters for H-bonds in water-glycerol solutions, the HBACF's for each H-bond can be compared at each concentration of glycerol to determine the relative dynamics of each H-bond. The H-bonds that tend to stay correlated for longer periods of time indicate a preferential configuration over other H-bonds. In order to compare the relaxation of different H-bond populations, the effects of the transient period and the exact H-bond criteria employed should be accounted for. As described previously, the extrapolated value of $c(0)$ describes the initial value of the H-bond population if the transient effects were excluded from the

relaxation of $c(t)$. If the values of $c(t)$ for different types of H-bonds are normalized to the extrapolated $c(0)$, then they can be directly compared.

By comparing the relative correlation times of different H-bonds at different glycerol concentrations in Figure 13, there are a few notable trends. First, the correlation time for w-w H-bonds is consistently shorter than the correlation time for other types of H-bonds. This is due to the consistently faster rates of H-bond breaking, k_b , for w-w H-bonds at all concentrations studied in Table 3. Because the correlation time for an H-bond pair is related to the likelihood of finding an H-bond pair in that configuration at a given time, this indicates that water oxygen atoms have a decreased probability of conforming to w-w H-bonds, especially at lower glycerol concentrations. Second, the correlation time of g-g H-bonds is similar, if only slightly shorter, than the correlation time of g-w H-bonds. This indicates little preference for glycerol oxygen atoms to conform to either g-g or g-w H-bonds. This adds insight into the original model used to predict the distribution of H-bonds in Figure 8. The original model assumed that an oxygen atom would have equal preference for donating to any acceptor oxygen. However, the dynamic analysis of H-bonds indicates that there is an increased probability of finding w-g H-bonds over w-w H-bonds and little difference between g-g and g-w H-bonds. The higher measured fraction of w-g and g-w H-bonds than predicted by the probability models can be explained by the faster H-bond dynamics of w-w H-bonds compared to w-g H-bonds.

4. Conclusions

By molecular dynamics simulations and extensive data analyses, we report new fundamental understandings to water-glycerol mixtures. First of all, by analyzing the concentration dependence of the fractions of H-bonds in water-glycerol mixtures, a maximum number of H-bonds occurring between opposite molecules occurs around 30 mol% glycerol. In addition, the observed maximum contribution of w-g and g-w H-bonds occurring around 30 mol% glycerol, is accepted to be responsible for the minimum and maximum properties observed for water-glycerol solutions at that water/glycerol golden ratio (30 mol% glycerol) [2, 3].

Secondly, to verify that the fractions of H-bonds measured are reliable and not only an artifact of the particular H-bond criteria used in this study, a probability model is used to account for entropic contributions and H-bond dynamics are used to account for non-equal probabilities of oxygen adhering to a particular H-bond conformation. The probability models developed show

that random association of oxygen atoms in the water-glycerol systems can account for a majority of the H-bond populations observed. However, the H-bonds that glycerol oxygen can form are dependent on the H-bonds that are formed by the other intramolecular glycerol oxygen. This limits the possible conformations of g-g H-bonds in the system and leads to a lower fraction of g-g H-bonds in the systems studied.

In addition, the comparison of H-bond dynamics indicates that w-w H-bonds decorrelate faster than other H-bonds in the system. This causes water oxygen to have a higher probability of conforming to w-g H-bonds than to w-w H-bonds and has the effect of increasing the fraction of w-g H-bonds in water-glycerol mixtures while decreasing fractions of w-w H-bonds.

Combining the predictions of the probability models and the H-bond dynamic analysis, the observed fractions of H-bonds provide a fundamental explanation to the water/glycerol golden ratio (30 mol% glycerol). The MD simulation and data mining procedures offer a general guideline to investigate systems where the hydrogen bond plays a critical role.

Acknowledgements

T. F., G. Z. and L.H. acknowledge the startup support from University of Oklahoma and partial support from the U.S. National Science Foundation (NSF) through grant CHE-1710102. Y.S. acknowledges the support from Swedish Research Council for Environment, Agricultural Sciences and Spatial Planning (Formas, Grant No. 2016-01098). We are very pleased to thank the OU Supercomputing Center for Education & Research (OSKER) at University of Oklahoma for their dedicated support.

Author Information

Corresponding Author

*E-mail: hll@ou.edu

ORCID: Liangliang Huang: [0000-0003-2358-9375](https://orcid.org/0000-0003-2358-9375)

Conflicts of interest

The authors declare no conflicts of interest.

Appendix

I. Numerical Evaluation of the Inverse Laplace Transform of the Autocorrelation Function

The inverse Laplace transform of $C(s)$ and its derivative back into the time domain are calculated using the Gaver-Stehfest method [42]:

$$x(t) \approx \frac{\ln(2)}{t} \sum_{i=1}^n V_i X\left(\frac{\ln(2)}{t} i\right) \quad (41)$$

With $X(s)$ corresponding to the Laplace transformation of a time dependent function $x(t)$. The number of summation terms, n , is a free parameter and is adjusted by trial and error. The best choice of n was found to be $10 \leq n \leq 14$ from ref. [43] and $14 \leq n \leq 16$ for the problems covered from ref. [44]. For the calculations in this study, n is selected to be 16. The term V_i is calculated by:

$$V_i = (-1)^{\binom{n}{\frac{n}{2}+1}} \sum_{k=\lfloor \frac{i+1}{2} \rfloor}^{\min(i, \frac{n}{2})} \frac{k^{\binom{n}{\frac{n}{2}+1}} (2k)!}{\binom{n}{\frac{n}{2}+k} k! (i-k)! (2k-1)!} \quad (42)$$

The choice of the Gaver-Stehfest method for numerically performing the inverse Laplace transform is based on the evaluation of different numerical inverse Laplace transform methods from ref. [44] where the method was shown to accurately model the analytical solutions for equations with exponential decay.

II. Switching between a non-switching function and a switching function implementation for calculating the Lennard-Jones interactions

All of the water-glycerol systems aside from the 70 mol% glycerol solution undergo structural equilibrations. For the 70 mol% glycerol solution, the system undergoes structural equilibration at 300K and 1 atm using the same simulation parameters specified in Sec. 2, but the Lennard-Jones potential is not calculated with a switching function as specified in Sec. 2.1. Instead, the Lennard-Jones interactions are calculated between atoms less than 12.0 Å apart and are 0 otherwise.

After approximately 70 ns of simulation time with the above conditions, the Lennard-Jones interactions are changed to adhere to the switching-function specified in Sec. 2.1. The average total energy of the system shows no signs of deviation over 5 ns after switching the method used to measure the Lennard-Jones interaction parameters. The average total energy over the 5 ns interval is -3656 eV with a relative standard deviation of 0.2%. Because the distance cutoffs used to directly calculate Lennard-Jones parameters are large, the Lennard-Jones potential already

evaluates close to 0 at near the cutoff radius. As a result, the energy contribution from pairs beyond the cutoff radius evaluated by the switching function are already close to 0. Atomic trajectories used for H-bond analysis for the 70 mol% glycerol solution are gathered after the Lennard-Jones switching function is implemented.

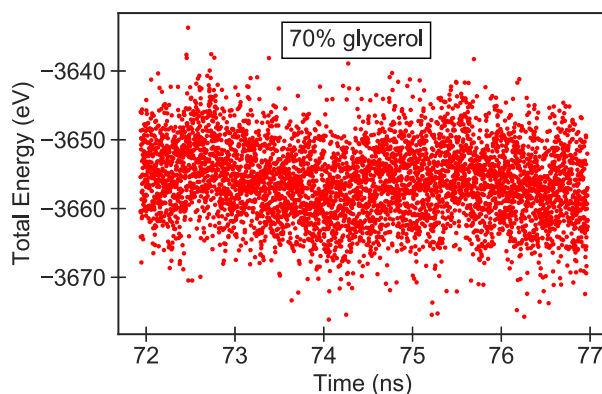


Figure A1. Total energy of the 70 mol% glycerol system shown for 5ns after changing the Lennard-Jones calculations from a non-switching function the switching function specified in Sec. 2.1. Time represents the total simulation time since the initial configuration.

III. Sensitivity Analysis of H-bond Dynamic and Diffusive Parameters

The estimated 95% confidence intervals for the dynamic and diffusive parameters listed in Table 3 are calculated from a Monte-Carlo sampling of the parameters. An interval is defined to randomly pick values for k_b , k_r , and τ_d . Then, the calculated value of $c(t)$ from equation (37) is compared to the measured values of $c(t)$. If more than 95% of the calculated values of $c(t)$ fall within the 95% confidence intervals of $c(t)$, then the pair of randomly selected variables is saved in a distribution. 400 pairs that satisfy the above criteria are generated and the top and bottom 2.5% of the values for k_b , k_r , and τ_d are eliminated from the distribution. The range between the maximum and minimum values for the distribution are compared to the interval allowed for the randomly generated parameters. If the range is greater than 65% of the range for the variables to be sampled, then the random sampling interval is increased and a new set of 400 parameters are generated until the range is less than 65% of the random sampling interval. This is to ensure that the random sampling interval is large enough to observe the middle 95% of the possible values for each parameter and not just a small portion of the distribution.

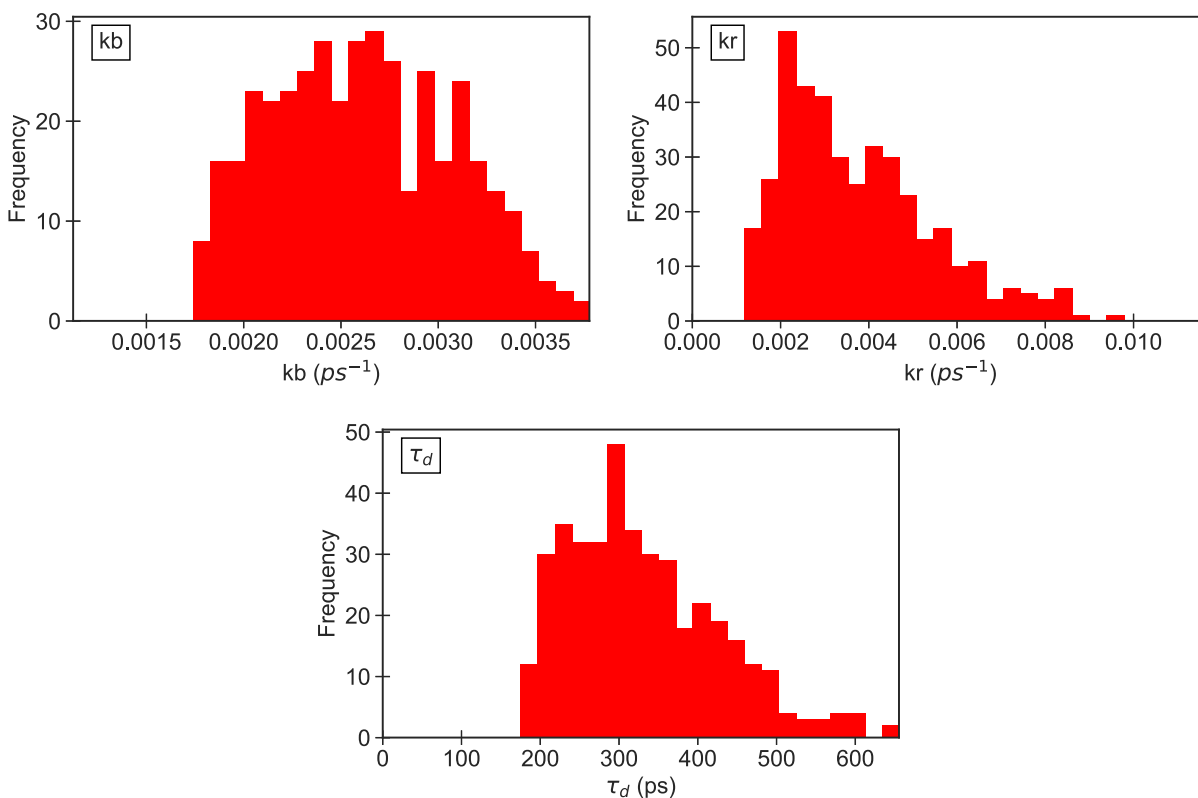


Figure A2. Distributions of 400 values of k_b , k_r , and τ_d used in equation (37) that fit the measured values of $c(t)$ for g - w H-bonds in a 30 mol% glycerol system. The ranges of the x-axis correspond to the allowed random sampling intervals.

A typical distribution of the values for k_b , k_r and τ_d is provided in Figure A2. Because values for the three parameters are generated in pairs, the 95% confidence intervals for each parameter are interdependent. This means that the distribution for one of the parameters is affected by the freedom to select values for the other two terms and still fit the measured values of $c(t)$. Also, it should be noted that not all of the distributions for the parameters are normally distributed. This would mean that the 95% confidence intervals would be different for the positive and negative deviations from the average values reported. However, the purpose of this sensitivity analysis is only to provide an approximation for the precision of the kinetic and diffusive parameters in Table 3, so the distributions are assumed to be normal enough to report identical positive and negative intervals from the average to approximate the middle 95% of the possible values of the parameters.

References

- [1] K. Murata and H. Tanaka, "Liquid-liquid transition without macroscopic phase separation in a water-glycerol mixture," *Nature Materials*, vol. 11, pp. 436-443, 2012.
- [2] L. B. Lane, "Freezing Points of Glycerol and Its Aqueous Solutions," *Industrial and Engineering Chemistry*, vol. 17, no. 9, p. 924, 1923.
- [3] A. Volk and C. J. Kähler, "Density model for aqueous glycerol solutions," *Experiments in Fluids*, vol. 59, no. 75, pp. 1-4, 2018.
- [4] C. Matta, L. Joly-Pottuz, M. I. De Barros Bouchet, J. M. Martin, M. Kano, Q. Zhang and W. A. Goddard III, "Superlubricity and tribochemistry of polyhydric alcohols," *Physical Review B*, vol. 78, p. 085436, 2008.
- [5] F. P. Bowden and D. Tabor, *The friction and lubrication of solids*, Clarendon Press, 1950.
- [6] C. Matta, O. L. Eryilmaz, M. I. De Barros Bouchet, A. Erdemir, J. M. Martin and K. Nakayama, "On the possible role of triboplasma in friction and wear of diamond-like carbon films in hydrogen-containing environments," *Journal of Physics D: Applied Physics*, vol. 42, p. 075307, 2009.
- [7] J. Teixeira, A. Luzar and S. Longeville, "Dynamics of hydrogen bonds: how to probe their role in the unusual properties of liquid water," *Journal of Physics: Condensed Matter*, vol. 18, pp. S2353-S2362, 2006.
- [8] J. Teixeira, "Dynamics of hydrogen bonds in water and consequences for the unusual behavior of supercooled water," *Pramana - Journal of Physics*, vol. 71, no. 4, pp. 761-768, 2008.
- [9] J. R. Errington and P. G. Debenedetti, "Relationship between structural order and the anomalies of liquid water," *Nature*, vol. 409, pp. 318-321, 2001.
- [10] D. A. Jahn, F. O. Akinkunmi and N. Giovambattista, "Effects of Temperature on the Properties of Glycerol: A Computer Simulation Study of Five Different Force Fields," *The Journal of Physical Chemistry B*, vol. 118, pp. 11284-11294, 2014.
- [11] D. A. Jahn, J. Wong, J. Bachler, T. Loerting and N. Giovambattista, "Glass polymorphism in glycerol-water mixtures: I. A computer simulation study," *Physical Chemistry Chemical Physics*, vol. 18, pp. 11042-11057, 2016.
- [12] J. L. Dashnau, N. V. Nucci, K. A. Sharp and J. M. Vanderkooi, "Hydrogen Bonding and the Cryoprotective Properties of Glycerol/Water Mixtures," *The Journal of Physical Chemistry B*, vol. 110, no. 27, pp. 13670-13677, 2006.
- [13] J. J. Towey, A. K. Soper and L. Dougan, "Preference for Isolated Water Molecules in a Concentrated Glycerol-Water Mixture," *The Journal of Physical Chemistry B*, vol. 115, pp. 7799-7807, 2011.
- [14] F. O. Akinkunmi, D. A. Jahn and N. Giovambattista, "Effects of Temperature on the Thermodynamic and Dynamical Properties of Glycerol-Water Mixtures: A Computer Simulation Study of Three Different Force Fields," *Journal of Physical Chemistry B*, vol. 119, pp. 6250-6261, 2015.
- [15] S. Plimpton, "Fast Parallel Algorithms for Short-Range Molecular Dynamics," *Journal of Computational Physics*, vol. 117, pp. 1-19, 1995.
- [16] *The URL for the LAMMPS website is <http://lammps.sandia.gov>.*

- [17] W. Shinoda, M. Shiga and M. Mikami, "Rapid estimation of elastic constant by molecular dynamics simulation under constant stress," *Physical Review B*, vol. 69, no. 13, p. 134103, 2004.
- [18] P. J. Steinbach and B. R. Brooks, "New spherical-cutoff methods for long-range forces in macromolecular simulation," *Journal of Computational Chemistry*, vol. 15, no. 7, 1994.
- [19] R. W. Hockney and J. W. Eastwood, *Computer Simulation Using Particles*, New York: Taylor & Francis Group, 1988.
- [20] J. L. F. Abascal and C. Vega, "A general purpose model for the condensed phases of water: TIP4P/2005," *The Journal of Chemical Physics*, vol. 123, p. 234505, 2005.
- [21] R. Chelli, P. Procacci, G. Cardini, R. G. Della Valle and S. Califano, "Glycerol condensed phases Part I. A molecular dynamics study," *Physical Chemistry Chemical Physics*, vol. 1, pp. 871-877, 1999.
- [22] W. D. Cornell, P. Cieplak, C. I. Bayly, I. R. Gould, K. M. Merz, D. M. Ferguson, D. C. Spellmeyer, T. Fox, J. W. Caldwell and P. A. Kollman, "A Second Generation Force Field for the Simulation of Proteins, Nucleic Acids, and Organic Molecules," *Journal of the American Chemical Society*, vol. 117, no. 19, pp. 5179-5197, 1995.
- [23] J. Blicek, F. Affouard, P. Bordat, A. Lerbret and M. Descamps, "Molecular dynamics simulations of glycerol glass-forming liquid," *Chemical Physics*, vol. 317, pp. 253-257, 2005.
- [24] J. Wuttke and W. Petry, "Structural relaxation in viscous glycerol: Coherent neutron scattering," *The Journal of Chemical Physics*, vol. 105, pp. 5177-5182, 1996.
- [25] L. Martínez, R. Andrade, E. G. Birgin and J. M. Martínez, "Packmol: A package for building initial configurations for molecular dynamics simulations," *Journal of Computational Chemistry*, vol. 30, no. 13, pp. 2157-2164, 2009.
- [26] L. W. Bosart and A. O. Snoddy, "Specific Gravity of Glycerol," *Industrial and Engineering Chemistry*, vol. 20, no. 12, pp. 1377-1379, 1928.
- [27] A. Luzar and D. Chandler, "Hydrogen-bond kinetics in liquid water," *Nature*, vol. 379, no. 4, pp. 55-57, 1996.
- [28] R. Olsen, B. Kvamme and T. Kuznetsova, "Hydrogen Bond Lifetimes and Statistics of Aqueous Mono-, Di-, and Tri-Ethylene Glycol," *AIChE Journal*, vol. 63, no. 5, pp. 1674-1689, 2017.
- [29] J. A. Padró, L. Saiz and E. Guàrdia, "Hydrogen bonding in liquid alcohols: a computer simulation study," *Journal of Molecular Structure*, vol. 416, pp. 243-248, 1997.
- [30] W. Danninger and G. Zundel, "Intense depolarized Rayleigh scattering in Raman spectra of acids caused by large proton polarizabilities of hydrogen bonds," *The Journal of Chemical Physics*, vol. 74, no. 5, pp. 2769-2777, 1981.
- [31] A. Mudalige and J. E. Pemberton, "Raman spectroscopy of glycerol/D2O solutions," *Vibrational Spectroscopy*, vol. 45, pp. 27-35, 2007.
- [32] R. Bergman and J. Swenson, "Dynamics of supercooled water in confined geometry," *Nature*, vol. 403, pp. 283-286, 2000.
- [33] A. Puzenko, Y. Hayashi, Y. E. Ryabov, I. Balin, Y. Feldman, U. Kaatzke and R. Behrends, "Relaxation Dynamics in Glycerol-Water Mixtures: I. Glycerol-Rich Mixtures," *The Journal of Physical Chemistry B*, vol. 109, pp. 6031-6035, 2005.

- [34] J. Teixeira and M.-C. Bellissent-Funel, "Experimental determination of the nature of diffusive motions of water molecules at low temperatures," *Physical Review A*, vol. 31, no. 3, pp. 1913-1917, 1985.
- [35] J. Wuttke, I. Chang, O. G. Randl, F. Fujara and W. Petry, "Tagged-particle motion in viscous glycerol: Diffusion-relaxation crossover," *Physical Review E*, vol. 54, no. 5, pp. 5364-5369, 1996.
- [36] A. Rahman and F. H. Stillinger, "Hydrogen-Bond Patterns in Liquid Water," *Journal of the American Chemical Society*, vol. 95, no. 24, pp. 7943-7948, 1973.
- [37] K. Yadav, "Hydrogen bond dynamics and vibrational spectral diffusion in aqueous solution of formaldehyde: a first principles molecular dynamics study," *Theoretical Chemistry Accounts*, vol. 137, no. 129, 2018.
- [38] A. Luzar, "Resolving the hydrogen bond dynamics conundrum," *Journal of Chemical Physics*, vol. 113, no. 23, pp. 10663-10675, 2000.
- [39] V. P. Voloshin and Y. I. Naberukhin, "Hydrogen Bond Lifetime Distributions In Computer-Simulated Water," *Journal of Structural Chemistry*, vol. 50, no. 1, pp. 78-89, 2009.
- [40] M. L. Antipova and V. E. Petrenko, "Hydrogen Bond Lifetime for Water in Classic and Quantum Molecular Dynamics," *Russian Journal of Physical Chemistry A*, vol. 87, no. 7, pp. 1170-1174, 2013.
- [41] P. Liu, E. Harder and B. J. Berne, "Hydrogen-Bond Dynamics in the Air-Water Interface," *The Journal of Physical Chemistry B*, vol. 109, pp. 2949-2955, 2005.
- [42] H. Stehfest, "Numerical Inversion of Laplace Transforms," *Communications of ACM*, vol. 13, no. 1, pp. 47-49, 1970.
- [43] S. T. Lee, M. C. H. Chien and W. E. Culham, "Vertical single-well pulse testing of a three-layer stratified reservoir," *SPE Annual Technical Conference and Exhibition*, 1984.
- [44] H. Hassanzadeh and M. Pooladi-Darvish, "Comparison of different numerical Laplace inversion methods for engineering applications," *Applied Mathematics and Computation*, vol. 189, pp. 1966-1981, 2007.
- [45] E. Arunan, G. R. Desiraju, R. A. Klein, J. Sadlej, S. Scheiner, I. Alkorta, D. C. Clary, R. H. Crabtree, J. J. Dannenberg, P. Hobza, H. G. Kjaergaard, A. C. Legon, B. Mennucci and D. J. Nesbitt, "Definition of the hydrogen bond (IUPAC Recommendations 2011)," *Pure and Applied Chemistry*, vol. 83, no. 8, pp. 1637-1641, 2011.
- [46] A. Stukowski, "Visualization and analysis of atomistic simulation data with OVITO - the Open Visualization Tool," *Modeling and Simulation in Materials Science and Engineering*, vol. 18, p. 015012, 2010.